Flexibility-Based Stress-Driven Nonlocal Frame Element: Formulation and Applications

Suchart Limkatanyu[*1,a], Worathep Sae-Long[2], Hamid M. Sedighi[3,4], Jaroon Rungamornrat[5], Piti Sukontasukkul[6], Hexin Zhang[7], and Prinya Chindaprasirt[8]

[1]*Department of Civil and Environmental Engineering, Faculty of Engineering, Prince of Songkla University, Songkhla 90112, Thailand*

[2]*Civil Engineering Program, School of Engineering, University of Phayao, Phayao 56000, Thailand*

[3]*Mechanical Engineering Department, Faculty of Engineering, Shahid Chamran University of Ahvaz, Ahvaz 6135783151, Iran*

[4]*Drilling Center of Excellence and Research Center, Shahid Chamran University of Ahvaz, Ahvaz 6135783151, Iran*

[5]*Applied Mechanics and Structures Research Unit, Department of Civil Engineering, Faculty of Engineering, Chulalongkorn University, Bangkok 10330, Thailand*

[6]*Construction and Building Materials Research Center, Department of Civil Engineering, King Mongkut's University of Technology North Bangkok, Bangkok 10800, Thailand*

[7]*School of Engineering and the Built Environment, Edinburgh Napier University, Edinburgh, Scotland EH10 5DT, UK*

[8]*Sustainable Infrastructure Research and Development Center, Department of Civil Engineering, Faculty of Engineering, Khon Kaen University, Khon Kaen 40002, Thailand*

The first author would like to dedicate this contribution to my beloved and influential teacher Professor Enrico Spacone on the occasion of his sixtieth birthday.

ABSTRACT

In the present work, a novel flexibility-based nonlocal frame element for size-dependent analyses of nano-sized frame-like structures is proposed. The material small-scale effect is consistently represented by the stress-driven nonlocal integral model and the element equation is constructed within the framework of flexibility-based finite element formulation. The merits of both stress-driven nonlocal integral model and flexibility-based finite element formulation render the proposed nonlocal frame element "*consistent*" and "*exact*". Therefore, the "*one-element-per-member*" modeling approach is applicable. The modified Tonti's diagram is utilized to show the overview of the element formulation and to summarize the formulation step. The element state determination process as well as the

[a]Corresponding author, Professor, E-mail: suchart.l@psu.ac.th

displacement recovery procedure are also discussed. Three numerical examples are employed to show accuracy, characteristics, and applications of the proposed nonlocal frame element. The first example shows the model capability to eliminate the "*constant-force*" paradoxical responses inherent to the Eringen's nonlocal frame model and the simplified strain-gradient frame model; the second presents and characterizes the essence of the material small-scale effect on global and local responses of a propped cantilever nanobeam; the third investigates the material small-scale effect on the tensile response of an auxetic metamaterial. All analysis results demonstrate that the material nonlocality associated with the stress-driven nonlocal integral model consistently yields a stiffer system response.

Keywords: nanoframe; stress-driven nonlocal elasticity; small-scale effect; flexibility-based frame element; finite element; auxetic metamaterials.

1. Introduction

In nanoscience and nanotechnology, frame-like structures have found a broad spectrum of novel applications such as atomic force microscopes [1-2], resonators [3-4], gyroscopes [5-6], actuators and sensors [7-8], auxetic metamaterials [9-11], and carbon nanotube networks [12-13]. Both experimental studies and atomistic/molecular dynamic simulations have confirmed the essence of the material small-scale effect on mechanical responses when the dimension of a structure ranges from nanoscale to microscale [14-19]. Long-range inter-atomic forces associated with the discrete nature of materials is responsible for the material small-scale effect inherent to nano-sized structures [20]. Classical (local) elasticity theory fails to represent the material small-scale effect since the discrete nature of materials cannot be homogenized into a continuum. The atomistic/molecular dynamic modeling approach could be a viable and natural choice to characterize mechanical responses of nano-sized structures [17-19], however, it is computationally expensive and time consuming. Therefore, only systems with small numbers of molecules and atoms can practically be analyzed using this approach [21]. To compromise between model accuracy and model efficiency, several researchers have enriched classical elasticity theory with the ability to account for the material small-scale effect, thus leading to a family of enhanced elasticity theories, such as strain gradient [16, 22-24], couple stress [25-28], and nonlocal elasticity models [29-32]. What all enhanced elasticity theories share is the addition of material length scales to characterize the material nonlocality associated with long-range inter-atomic forces. As the most popular among these enhanced elasticity theories, the strain-driven nonlocal theory proposed by Eringen [29] considers the material small-scale effect through an integral convolution statement between the strain fields and a scalar kernel function representing the material nonlocality. Consequently, the essence of this nonlocal theory is in its assertion that the stress at a given point is induced not merely by the strain at a particular point but also by strains at all other points throughout the elastic body. It worth remarking that Vaccaro et al. [33] has recently adopted the essence of Eringen nonlocal theory [29] to develop a rational nonlocal elastic foundation model and named it the displacement-driven nonlocal foundation model. Different structural-mechanics models have cooperated with this nonlocal theory to include the material small-scale effect [34-42]. However, several researchers have noticed peculiar responses obtained with these small-scale structural-mechanics models and considered them as a “paradox” [43-46]. Romano et al. [47]

diagnosed the root of this paradox and concluded that adoption of the strain-driven nonlocal theory could lead to an ill-posed structural-mechanics problem. Furthermore, Vaccaro et al. [48] clearly demonstrated that the bending moment response obtained with the strain-driven nonlocal beam model does not satisfy differential and boundary equilibrium conditions, thus providing a physical insight into the ill-posed structural-mechanics problem. As a result, several researchers have recently turned their focus from the strain-driven nonlocal model to the strain-gradient-type constitutive model as an alternative to develop rational structural-mechanics models [23-24, 49-53]. In essence, the strain-gradient-type constitutive model asserts that the stress at a generic point is induced not only by the strain but also by the derivatives of the strain (strain-gradient). The strain-gradient structural-mechanics models was proven to be well-posed within the framework of variational formulation by Niiranen et al. [54]. However, non-classical boundary conditions associated with the higher-order governing differential equation usually occur for strain-gradient structural-mechanics models and there is no consensus on their physical meaning. As a result, different views on the non-classical boundary conditions could alter obtained responses [53].

By interchanging source and output quantities of the strain-driven nonlocal integral constitutive model, Romano and Barretta [31] developed an innovative nonlocal integral constitutive model and named it the "stress-driven" nonlocal constitutive model. The basis of this innovative nonlocal model is in its affirmation that the strain at a reference point depends not only on the stress at a particular point but also on stresses at all other points throughout the elastic body. As shown by Romano and Barretta [55] and Apuzzo et al. [56], the stress-driven nonlocal constitutive model leads to a well-posed structural-mechanics problem. To ease the model application, the consequent differential form of the stress-driven nonlocal constitutive model was consistently derived by Romano and Barretta [31] and Vaccaro et al. [57]. Although the resulting governing differential equation possesses the higher-order derivative term, the necessity of the additional boundary condition is satisfied by the supplementary constitutive boundary condition. Also, unlike in strain-gradient structural-mechanics models, there is no ambiguity in the non-classical boundary condition. Consequently, researchers worldwide have recently adopted the stress-driven nonlocal constitutive law both in the integro-differential form and the equivalent differential form to develop reliable structural-mechanics models for characterization of nano-sized structures [58-65].

In literature, nonlocal finite element models have been formulated by several researchers [34, 36, 39, 66-70] and have been mainly applied to single nano-sized bars and beams. Most of them have adopted the differential form of the strain-driven nonlocal model, thus resulting in paradoxical and inconsistent responses in some cases. To remedy these problematic responses, the integro-differential form of the strain-driven nonlocal model has recently been revisited by several researchers and the stiffness-based finite element formulation has been employed to construct the model equation [66-69]. Due to the approximate nature of assumed displacement interpolation functions, a large number of elements are usually required to obtain a converged solution even for a simple beam system [67-69]. Furthermore, a special element assembly procedure is required to account for the material nonlocality throughout the domain and the resulting structural stiffness matrix is fully populated, thus increasing the computational expense [67-69]. It is worth remarking that besides the nonlocal finite element method, the so-called "*nonlocal operator*" method proposed by Rabczuk et al. [71] and Ren et al. [72] has recently been employed to characterize nano-sized structures [73-74]. This innovative numerical method was originally developed for solving partial differential equations of field problems (e.g. solid mechanics, electromagnetics) and is consistent with the method of weighted residuals and the principle of variation.

To narrow the research gap in the area of nonlocal finite element models, the development of a rational nonlocal frame model with computational efficiency is sought. As mentioned by Numanoglu and Civalek [75] and Russillo et al. [76], nano-sized skeleton structures have found a wide spectrum of novel applications in nanoscience and nanotechnology: auxetic metamaterials [9-11], carbon nanotube networks [12-13], cellular nanostructures [77], and electro-thermal actuator bent-beams [78]. An efficient nonlocal frame model plays an essential role in modeling and characterizing responses of these nano-sized skeleton structures. Up to now, only a few nonlocal frame models have been proposed in the research community [75-76, 79]. For example, Numanoglu and Civalek [75] developed a nonlocal frame element based on Eringen's nonlocal differential model and the Galerkin weighted residual method. Hozhabrossadati et al. [79] also employed Eringen's nonlocal differential model and the Galerkin weighted residual method to construct a nonlocal grillage element. It is worth emphasizing that Eringen's nonlocal differential model is adopted by Numanoglu and Civalek [75] and Hozhabrossadati et al. [79] to develop their nonlocal frame models. Therefore, paradoxical and inconsistent responses can possibly be

obtained with these nonlocal frame models. Recently, Russillo et al. [76] proposed a "paradox-free" nonlocal frame element. In this element formulation, exact displacement interpolation functions were obtained from the homogeneous solution to the stress-driven nonlocal differential equilibrium equation, thus yielding the "exact" element stiffness matrix as well as the "exact" element mass matrix. However, the focus of the study was mainly on vibration analyses of nano-sized frames and the general framework of the finite element formulation was not thoroughly presented. Therefore, there is still room to add a rational nonlocal frame element into the research community and hence the primary interest of the present work.

The nonlocal frame model proposed in the present work is a marriage of the stress-driven nonlocal integral model and the flexibility-based finite element formulation. It is observed that the deformation-force relation (compliance form) in the stress-driven nonlocal integral model is very well suited to the nature of flexibility-based finite element formulation. Furthermore, the element load can be added naturally within the framework of flexibility-based finite element formulation and this feature is not valid in the stiffness-based finite element formulation employed by Russillo et al. [76]. To date, the flexibility-based finite element formulation has been extensively employed to develop a more computationally efficient numerical platform for nonlinear analysis of structures [80-84]. Several drawbacks inherent in the standard stiffness-based finite element formulation were shown to be eliminated in the flexibility-based finite element formulation [80]. The enhanced accuracy of the flexibility-based model is associated with the merit of employed force interpolation functions. This merit relies on the fact that the internal force distributions along the element length can be exactly determined even for the nonlocal material, thus leading to the "exact" finite element model. Therefore, the "one-element-per-member" modeling approach is valid for the proposed nonlocal frame element. To the authors' best knowledge, the present work proposes for the first time the flexibility-based stress-driven nonlocal frame model. The advantages of both stress-driven nonlocal integral model and flexibility-based finite element formulation are fully considered by the proposed frame model.

The structure of this research work is as follows: first, the stress-driven nonlocal integral constitutive models for axial and bending responses are introduced. Then, the theoretical framework of flexibility-based finite element formulation is discussed and the flexibility-based stress-driven nonlocal frame model is formulated within the framework of the matrix virtual force

principle. The modified Tonti's diagram is utilized to show the overview of the model formulation. The element state determination process as well as the displacement recovery procedure are also presented. Finally, an assessment of model accuracy and a demonstration of model application and effectiveness are conducted via three numerical examples. The first example shows the model capability to eliminate the "constant-force" paradoxical responses inherent to the Eringen's nonlocal frame model [34, 37] and the simplified strain-gradient frame model [52-53]. The second presents and characterizes the essence of the material small-scale effect on global and local responses of a propped cantilever nanobeam. The third investigates the material small-scale effect on the tensile response of an auxetic metamaterial. It is worth emphasizing that every frame member in all examples is represented only by a single proposed frame element, thus requiring no finite-element discretization. The proposed frame element is implemented in the general-purpose finite element platform FEAP [85].

2. Stress-Driven Nonlocal Integral Model: Axial and Bending Responses

The stress-driven nonlocal integral model proposed by Romano and Barretta [31] is employed in this study to represent the small-scale characteristic present in nano-sized structures. In this nonlocal model, the strain at a point is induced by stresses at all points throughout the domain via a convolution integral statement. For the present emphasis of a planar Euler-Bernoulli frame, the expressions of the stress-driven nonlocal models for axial and bending responses are given by Barretta et al. [59] and Vaccaro et al. [48], respectively as:

$$\varepsilon(x) = \int_L \psi\left(|x-\bar{x}|, l_c\right) \frac{N(\bar{x})}{E_{xx}(\bar{x}) A(\bar{x})} d\bar{x} \tag{1}$$

$$\kappa(x) = \int_L \psi\left(|x-\bar{x}|, l_c\right) \frac{M(\bar{x})}{E_{xx}(\bar{x}) I(\bar{x})} d\bar{x} \tag{2}$$

where $\varepsilon(x)$ $\kappa(x)$ $N(\bar{x})$ and bending moment $M(\bar{x})$; $E_{xx}(\bar{x})$ is the elastic modulus; $A(\bar{x})$ is the section area; $I(\bar{x})$ is the second moment of area; L is the frame length; $\psi\left(|x-\bar{x}|, l_c\right)$

nonlocality; $|x-\bar{x}|$ is the Euclidean distance between two material points x and $\bar{x}$; and l_c is the nonlocal characteristic length.

In this study, the following Helmholtz bi-exponential function is adopted as a scalar kernel function:

$$\psi_H\left(|x-\bar{x}|, l_c\right)=\frac{1}{2l_c}e^{-\frac{|x-\bar{x}|}{l_c}} \tag{3}$$

As shown by Barretta et al. [62], the Helmholtz bi-exponential function of Eq. (3) satisfies the following properties:

$$\psi_H\left(x, l_c\right)=\psi_H\left(-x, l_c\right)\geq 0 : \textit{parity-positivity-symmetry} \tag{4}$$

$$\lim_{l_c\to 0^+}\psi_H\left(x, l_c\right)=\delta\left(x\right) : \textit{limit impulsivity} \tag{5}$$

$$\lim_{l_c\to 0^+}\int_{-\infty}^{+\infty}\psi_H\left(|x-\bar{x}|, l_c\right)f\left(\bar{x}\right)d\bar{x}=f\left(x\right) \tag{6}$$

The implication of Eq. (4) ensures that the employed scalar kernel function is a positive distance decaying function and attains its maxima at $x=\bar{x}$ while the requirements of Eqs. (5) and (6) ensure that the integro-differential constitutive relations of Eqs. (1) and (2) become the local compliance constitutive relations when the nonlocal characteristic length l_c approaches zero ($l_c\to 0^+$). It is worth mentioning that Barretta et al. [59] and Romano and Barretta [31] consistently transformed the integral convolution of Eqs. (1) and (2) into equivalent differential forms by employing the Helmholtz bi-exponential function of Eq. (3) as the scalar kernel function. The present study gains particular merit of this achievement since the constitutive relation in the differential form can be applied with ease and the analytical solution to the problem can be obtained. This feature is crucial to the verification and assessment of the proposed numerical model. Besides the Helmholtz bi-exponential function, other functions such as Gaussian, modified Bessel can be used as a scalar kernel function as long as they satisfy the requirements of Eqs. (4), (5), and (6).

For the ease of the subsequent model formulation, the integro-differential constitutive relations of Eqs. (1) and (2) are written in the matrix form as:

$$\mathbf{d}\left(x\right)=\int_L \boldsymbol{\psi}_H\left(|x-\bar{x}|, l_c\right)\mathbf{f}\left(\bar{x}\right)\mathbf{D}\left(\bar{x}\right)d\bar{x} \tag{7}$$

where the vector $\mathbf{d}(x)=\lfloor \varepsilon(x) \quad \kappa(x) \rfloor^T$ collects the frame section deformations; the vector $\mathbf{D}(\bar{x})=\lfloor N(\bar{x}) \quad M(\bar{x}) \rfloor^T$ compiles the frame section forces; the diagonal matrix $\mathbf{f}(\bar{x})=dia\left[\frac{1}{E_{xx}(\bar{x})A(\bar{x})} \quad \frac{1}{E_{xx}(\bar{x})I(\bar{x})}\right]$ collects the frame section flexibility coefficients; and the diagonal matrix $\boldsymbol{\psi}_H\left(|x-\bar{x}|, l_c\right)=dia\left[\frac{1}{2l_c}e^{-\frac{|x-\bar{x}|}{l_c}} \quad \frac{1}{2l_c}e^{-\frac{|x-\bar{x}|}{l_c}}\right]$ contains the scalar kernel function.

3. Flexibility-Based Nonlocal Frame Formulation

3.1 Equilibrium

3.1.1 Strong form

A nonlocal simply-supported frame under end loads (Q_1, Q_2, and Q_3) and distributed loads ($w_x(x)$ and $w_y(x)$) is shown in Fig. 1a. For the sake of simplicity, axially and vertically distributed loads are assumed uniform along the whole length of the frame ($w_x(x)=w_{x0}$ and $w_y(x)=w_{y0}$). However, the model formulation is also valid for the case of non-uniformly distributed loads.

A differential segment *dx* taken from the frame is shown in Fig. 1b. Considering all equilibriums of this differential segment provides the following relations:

$$\frac{dN(x)}{dx}+w_{x0}=0 \tag{8}$$

$$\frac{dV(x)}{dx}-w_{y0}=0 \tag{9}$$

$$\frac{dM(x)}{dx}+V(x)=0 \tag{10}$$

Based on the Euler-Bernoulli beam hypothesis, the shear force $V(x)$ plays no role in the model formulation and can be eliminated by combining Eqs. (9) and (10) into a single expression as:

$$\frac{d^2M(x)}{dx^2}+w_{y0}=0 \tag{11}$$

For the sake of conciseness, equilibrium conditions of Eqs. (8) and (11) are written in the matrix form as:

$$\mathbf{L}^T\mathbf{D}(x)+\mathbf{w}=0 \tag{12}$$

where $\mathbf{w}=\lfloor w_{x0} \quad w_{y0} \rfloor^T$ represents the element load vector; and the diagonal matrix $\mathbf{L}=dia\left[\frac{d}{dx} \quad \frac{d^2}{dx^2}\right]$ contains differential operators.

3.1.2 Force interpolation functions

Within the framework of flexibility-based finite element model, the nonlocal frame element is formulated. In this type of finite element formulation, the element section forces $\mathbf{D}(x)$ are considered as primary variables and must satisfy the equilibrium requirement of Eq. (12) in the point-wise sense. To fulfill this requirement, equilibrated force interpolations are necessary and their derivation is to be presented hereafter.

The nonlocal simply-supported frame of Fig 1a with its support reactions is shown in Fig 2a. Considering all equilibriums of the cut frame segment shown in Fig. 2b yields the following internal-external force relations.

$$N(x)=Q_1+(L-x)w_{x0} \tag{13}$$

$$M(x)=Q_2\left(-1+\frac{x}{L}\right)+Q_3\left(\frac{x}{L}\right)+\left(\frac{Lx}{2}-\frac{x^2}{2}\right)w_{y0} \tag{14}$$

It is worth emphasizing that the internal-external force relations of Eqs. (13) and (14) respectively satisfy the differential equilibrium conditions of Eqs. (8) and (11), thus fulfilling the fundamental requirement of the flexibility-based finite element model.

In the matrix form, Eqs. (13) and (14) can be expressed together as:

$$\mathbf{D}(x)=\mathbf{N}_{\mathbf{Q}}(x)\mathbf{Q}+\mathbf{N}_{\mathbf{w}}(x)\mathbf{w} \tag{15}$$

where the vector $\mathbf{Q}=\lfloor Q_1 \quad Q_2 \quad Q_3 \rfloor^T$ contains element nodal forces associated with the simply-supported system; and the force-interpolation matrices $\mathbf{N}_{\mathbf{Q}}(x)$ and $\mathbf{N}_{\mathbf{w}}(x)$ are defined as:

$$\mathbf{N}_{\mathbf{Q}}(x)=\begin{bmatrix}1 & 0 & 0\\ 0 & -1+x/L & x/L\end{bmatrix} \text{ and } \mathbf{N}_{\mathbf{w}}(x)=\begin{bmatrix}L-x & 0\\ 0 & x(L-x)/2\end{bmatrix} \tag{16}$$

In literature, the element nodal forces $Q_1,\ Q_2, \text{and}\ Q_3$ are known as basic forces and are associated with the system without rigid-body modes (the basic system). It is worth mentioning that exclusion of all rigid-body modes from the system kinematics is necessary for establishing the equilibrated internal-external force relations of Eqs. (13) and (14). Besides the simply-supported system, the clamped-free (cantilever) system can be also employed a basic system. Details on this issue are thoroughly discussed in Elias [86].

3.2 Section Constitutive Relation: Stress-Driven Nonlocal Integral Model

In the case of a prismatic frame with homogeneous material ($E_{xx}(\overline{x})A(\overline{x}) = E_{xx}A$ and $E_{xx}(\overline{x})I(\overline{x}) = E_{xx}I$), the matrix nonlocal constitutive relation of Eq. (7) can be written in the form similar to that of the local frame model as:

$$\mathbf{d}(x)=\mathbf{f}\,\mathbf{D}^{NL}(x) \tag{17}$$

where $\mathbf{D}^{NL}(x)$ represents the nonlocal section force vector and is defined as:

$$\mathbf{D}^{NL}(x)=\int_L \boldsymbol{\psi}_H\left(|x-\overline{x}|,\, l_c\right)\mathbf{D}(\overline{x})\,d\overline{x}=\mathbf{N}_{\mathbf{Q}}^{NL}(x)\mathbf{Q}+\mathbf{N}_{\mathbf{w}}^{NL}(x)\mathbf{w} \tag{18}$$

with $\mathbf{N}_{\mathbf{Q}}^{NL}(x)$ and $\mathbf{N}_{\mathbf{w}}^{NL}(x)$ being defined as:

$$\begin{aligned}\mathbf{N}_{\mathbf{Q}}^{NL}(x)&=\int_L \boldsymbol{\psi}_H\left(|x-\overline{x}|,\, l_c\right)\mathbf{N}_{\mathbf{Q}}(\overline{x})\,d\overline{x}\\ \mathbf{N}_{\mathbf{w}}^{NL}(x)&=\int_L \boldsymbol{\psi}_H\left(|x-\overline{x}|,\, l_c\right)\mathbf{N}_{\mathbf{w}}(\overline{x})\,d\overline{x}\end{aligned} \tag{19}$$

As observed in Eq. (17), the flexibility form of the section constitutive relation confirms that the stress-driven nonlocal integral model is very well suited and natural to the flexibility-based finite frame formulation. The section constitutive relation of Eq. (17) together with the internal-external force relation of Eq. (16) enable the expression of the section deformations $\mathbf{d}(x)$ in terms of the external forces $\mathbf{Q}$ and $\mathbf{w}$ via the convolution integration.

3.3 Compatibility: Element Flexibility Equation

In a scalar approach to structural-mechanics problems, the compatibility condition can be written in an alternative manner using the virtual force principle. The fundamental expression of the virtual force equation is:

$$\delta W^* = \delta W^*_{int} + \delta W^*_{ext} = 0 \tag{20}$$

where δW^* is the total complementary virtual work; δW^*_{int} the internal complementary virtual work; and δW^*_{ext} the external complementary virtual work.

In the present interest of the nonlocal simply-supported frame shown in Fig. 1a, δW^*_{int} and δW^*_{ext} can be defined as:

$$\delta W^*_{int} = \int_L \delta \mathbf{D}^T(x)\mathbf{d}(x)\,dx \tag{21}$$

$$\delta W^*_{ext} = -\int_L \delta \mathbf{w}^T(x)\mathbf{u}(x)\,dx - \delta \mathbf{Q}^T\mathbf{V} \tag{22}$$

where $\mathbf{V} = \lfloor V_1 \quad V_2 \quad V_3 \rfloor^T$ represents the basic element deformation vector and its conjugate-work vector is the basic element force vector $\mathbf{Q}$.

The virtual element distributed load vector $\delta\mathbf{w}(x)$ can be arbitrarily chosen to be zero without loss of model generality. Therefore, the virtual force relation of Eq. (20) becomes:

$$\int_L \delta \mathbf{D}^T(x)\mathbf{d}(x)\,dx - \delta \mathbf{Q}^T\mathbf{V} = 0 \tag{23}$$

Eq. (23) describes the compatibility relation between the section deformations $\mathbf{d}(x)$ and the basic element deformations $\mathbf{V}$ through the integral statement with the aid of an equilibrated virtual force system ($\delta\mathbf{D}(x)$ and $\delta\mathbf{Q}$).

Substituting Eqs. (17) and (16) into Eq. (23) and accounting for the arbitrariness of $\delta\mathbf{Q}$ provide the following element flexibility relation:

$$\overline{\mathbf{F}}^{NL}\mathbf{Q} + \mathbf{V}^{NL}_{\mathbf{w}} = \mathbf{V} \tag{24}$$

where $\bar{\mathbf{F}}^{NL} = \int_L \mathbf{N}_{\mathbf{Q}}^T(x)\mathbf{f}\,\mathbf{N}_{\mathbf{Q}}^{NL}(x)\,dx$ is the nonlocal element flexibility matrix; and $\mathbf{V}_{\mathbf{w}}^{NL} = \left(\int_L \mathbf{N}_{\mathbf{Q}}^T(x)\mathbf{f}\,\mathbf{N}_{\mathbf{w}}^{NL}(x)\,dx\right)\mathbf{w}$ collects the basic element deformations due to the applied uniform distributed loads $\mathbf{w} = \lfloor\, w_{x0} \quad w_{y0} \,\rfloor^T$.

Equilibrium of Eq. (15), compatibility relation of Eq. (24), and constitutive relation of Eq. (17) establish a complete set of basic ingredients required for the flexibility-based nonlocal frame formulation and are summarized in the modified Tonti's diagram of Fig. 3 [87].

The inversion of the element flexibility relation of Eq. (24) yields the basic element stiffness relation as:

$$\mathbf{Q} + \mathbf{Q}_{\mathbf{w}} = \bar{\mathbf{K}}^{NL}\mathbf{V} \tag{25}$$

where the matrix $\bar{\mathbf{K}}^{NL} = \left[\bar{\mathbf{F}}^{NL}\right]^{-1}$ represents the basic element stiffness matrix; and the vector $\mathbf{Q}_{\mathbf{w}} = \bar{\mathbf{K}}^{NL}\mathbf{V}_{\mathbf{w}}^{NL} = \lfloor\, w_{x0}L \quad -w_{y0}L^2/12 \quad w_{y0}L^2/12 \,\rfloor^T$ collects the basic element forces associated with the uniformly distributed loads (w_{x0} and w_{y0}). It is worth noting that these basic element forces are the same as those obtained for the local frame model due to statical determinacy of the simply-supported system. Therefore, the superscript *NL* appended to the vector $\mathbf{Q}_{\mathbf{w}}$ can be dropped.

3.4 Rigid-Body Mode Transformation

To cooperate with the flexibility-based nonlocal frame model in the framework of stiffness-based finite element platform, injection of all rigid-body modes into the simply-supported system (the basic system) of Fig. 1a is required. This rigid-body-mode injection can be achieved through the rigid-body-mode transformation matrix $\mathbf{\Gamma}_{RBM}$. The statical and kinematical relations between the systems with and without rigid-body modes as shown in Fig. 4 give the following transformation expressions:

$$\mathbf{P} = \mathbf{\Gamma}_{RBM}^T\mathbf{Q} + \mathbf{P}_{\mathbf{w}} \tag{26}$$

$$\mathbf{V} = \mathbf{\Gamma}_{RBM}\mathbf{U} \tag{27}$$

where the vector $\mathbf{P} = \lfloor P_1 \quad P_2 \quad P_3 \quad P_4 \quad P_5 \quad P_6 \rfloor^T$ is the element force vector associated with the system with rigid-body modes (the complete system) and the vector $\mathbf{U} = \lfloor U_1 \quad U_2 \quad U_3 \quad U_4 \quad U_5 \quad U_6 \rfloor^T$ is its conjugate-work displacement vector; the vector $\mathbf{P}_\mathbf{w} = \lfloor -w_{x0}L \quad w_{y0}L/2 \quad 0 \quad 0 \quad w_{y0}L/2 \quad 0 \rfloor^T$ collects the element forces required to equilibrate with the uniformly distributed loads (w_{x0} and w_{y0}); and the rigid-body-mode transformation matrix $\mathbf{\Gamma}_{RBM}$ is defined as:

$$\mathbf{\Gamma}_{RBM} = \begin{bmatrix} -1 & 0 & 0 & 1 & 0 & 0 \\ 0 & 1/L & 1 & 0 & -1/L & 0 \\ 0 & 1/L & 0 & 0 & -1/L & 1 \end{bmatrix} \tag{28}$$

Based on Eqs. (25), (26), and (27), the complete element stiffness equation is:

$$\mathbf{P} = \mathbf{K}^{NL}\mathbf{U} + \mathbf{F}_\mathbf{w} \tag{29}$$

where $\mathbf{K}^{NL} = \mathbf{\Gamma}_{RBM}^T \bar{\mathbf{K}}^{NL} \mathbf{\Gamma}_{RBM}$ is the complete element stiffness matrix (congruent transformation); and $\mathbf{F}_\mathbf{w} = -\mathbf{\Gamma}_{RBM}^T \mathbf{Q}_\mathbf{w} + \mathbf{P}_\mathbf{w}$ is the element force vector due to the presence of the uniformly distributed loads (w_{x0} and w_{y0}) and is simply equal to that obtained for the local frame model.

4. Element State Determination

For nonlinear analyses of frame structures, the flexibility-based frame model requires a special procedure to compute the element resisting forces and element stiffness matrix. Several researchers have proposed different element state determination procedures for nonlinear flexibility-based frame models. For the present study of linear structural analyses, the flexibility-based element state determination becomes much simpler and is explained following the framework of the procedure proposed by Limkatanyu and Spacone [88]. All integrations required in the element state determination are computed numerically using the Gauss-Lobatto quadrature. The merit of the Gauss-Lobatto quadrature is that the element ends are included in the integration points. Therefore, the extrapolation process to obtain element-end forces and deformations is not required like in the Gauss-Legendre quadrature. The step-by-step procedure of the element state determination is presented as follows:

I. At each integration point i ($\xi_i = x_i / L$), perform the convolution integrations of Eq. (19) numerically to compute the nonlocal force-interpolation matrices $\mathbf{N}_{\mathbf{Q}}^{NL}\left(\xi_i\right)$ and $\mathbf{N}_{\mathbf{w}}^{NL}\left(\xi_i\right)$:

$$\mathbf{N}_{\mathbf{Q}}^{NL}\left(\xi_i\right) = J\sum_{j=1}^{N_{GL}} w_j \boldsymbol{\psi}_H\left(\left|\xi_i - \overline{\xi}_j\right|, l_c\right)\mathbf{N}_{\mathbf{Q}}\left(\overline{\xi}_j\right)$$

$$\mathbf{N}_{\mathbf{w}}^{NL}\left(\xi_i\right) = J\sum_{j=1}^{N_{GL}} w_j \boldsymbol{\psi}_H\left(\left|\xi_i - \overline{\xi}_j\right|, l_c\right)\mathbf{N}_{\mathbf{w}}\left(\overline{\xi}_j\right)$$

where $J = L/2$ is the Jacobian for $\xi, \overline{\xi} \in [-1, 1]$; w_j is the weight function at integration point j ($\overline{\xi}_j = \overline{x}_j / L$); and N_{GL} is the number of integration points.

II. Compute the element flexibility matrix $\overline{\mathbf{F}}^{NL}$ and the basic element deformations $\mathbf{V}_{\mathbf{w}}^{NL}$ due to the element loads **w**:

$$\overline{\mathbf{F}}^{NL} = J\sum_{i=1}^{N_{GL}} w_i \mathbf{N}_{\mathbf{Q}}^{T}\left(\xi_i\right)\mathbf{f}\mathbf{N}_{\mathbf{Q}}^{NL}\left(\xi_i\right)$$

$$\mathbf{V}_{\mathbf{w}}^{NL} = J\left(\sum_{i=1}^{N_{GL}} w_i \mathbf{N}_{\mathbf{Q}}^{T}\left(\xi_i\right)\mathbf{f}\,\mathbf{N}_{\mathbf{w}}^{NL}\left(\xi_i\right)\right)\mathbf{w}$$

III. Invert the element flexibility matrix $\overline{\mathbf{F}}^{NL}$ to obtain the basic element stiffness matrix $\overline{\mathbf{K}}^{NL} = \left[\overline{\mathbf{F}}^{NL}\right]^{-1}$.

IV. Compute the basic element forces associated with the element loads **w**:

$$\mathbf{Q}_{\mathbf{w}} = \overline{\mathbf{K}}^{NL}\mathbf{V}_{\mathbf{w}}^{NL}$$

As mentioned previously, these basic element forces are identical to those obtained for the local frame model due to statical determinacy of the simply-supported system. Therefore, this step can be skipped. However, the computed basic element forces $\mathbf{Q}_{\mathbf{w}} = \overline{\mathbf{K}}^{NL}\mathbf{V}_{\mathbf{w}}^{NL}$ can be employed to verify the accuracy of the basic element stiffness matrix $\overline{\mathbf{K}}^{NL}$ and basic element deformations $\mathbf{V}_{\mathbf{w}}^{NL}$ determined numerically in step II.

V. Construct the complete element stiffness equation from the basic stiffness equation using the rigid-body-mode transformation:

$$\mathbf{P} = \mathbf{K}^{NL}\mathbf{U} + \mathbf{F}_{\mathbf{w}}$$

where $\mathbf{K}^{NL} = \mathbf{\Gamma}_{RBM}^{T} \bar{\mathbf{K}}^{NL} \mathbf{\Gamma}_{RBM}$ and $\mathbf{F}_{\mathbf{w}} = -\mathbf{\Gamma}_{RBM}^{T} \mathbf{Q}_{\mathbf{w}} + \mathbf{P}_{\mathbf{w}}$.

VI. Once the element nodal displacements **U** are obtained, the basic element deformations **V** and basic element forces **Q** can be obtained as:

$$\mathbf{V} = \mathbf{\Gamma}_{RBM} \mathbf{U} \text{ and } \mathbf{Q} + \mathbf{Q}_{\mathbf{w}} = \bar{\mathbf{K}}^{NL} \mathbf{V}$$

VII. The nonlocal sectional forces $\mathbf{D}^{NL}\left(\xi_i\right)$ at integration point *i* can be computed as:

$$\mathbf{D}^{NL}\left(\xi_i\right) = \mathbf{N}_{\mathbf{Q}}^{NL}\left(\xi_i\right)\mathbf{Q} + \mathbf{N}_{\mathbf{w}}^{NL}\left(\xi_i\right)\mathbf{w}$$

VIII. The sectional deformations $\mathbf{d}\left(\xi_i\right)$ at integration point *i* can be obtained as:

$$\mathbf{d}\left(\xi_i\right) = \mathbf{f}\,\mathbf{D}^{NL}\left(\xi_i\right)$$

5. Displacement Recovery Procedure

Within the framework of flexibility-based finite element formulation, the axial-displacement $u\left(x\right)$ and vertical-displacement $v\left(x\right)$ fields cannot be determined in a direct manner since there is no displacement interpolation function required in the formulation process. This is in opposition to the stiffness-based finite element formulation in which the displacement fields are related to nodal displacements through the displacement interpolation functions. Therefore, integrations of the following compatibility relations are required to recover the axial-displacement $u\left(x\right)$ and vertical-displacement $v\left(x\right)$ fields:

$$\varepsilon\left(x\right) = \frac{du\left(x\right)}{dx} \text{ and } \kappa\left(x\right) = \frac{d^2 v\left(x\right)}{dx^2} \tag{30}$$

Sectional deformations ($\varepsilon\left(x\right)$ and $\kappa\left(x\right)$) at N_{GL} integration points can be obtained using the nonlocal constitutive relation of Eq. (17) and are collected in terms of N_{GL} axial-strain and bending-curvature values as $\varepsilon_j = \boldsymbol{\varepsilon}\left(\xi_j\right)$ and $\kappa_j = \boldsymbol{\kappa}\left(\xi_j\right)$ where $\xi_j = x_j / L$ represents a natural coordinate. Using the Lagrange interpolation technique, the axial-strain $\varepsilon\left(x\right)$ and bending-curvature $\kappa\left(x\right)$ fields can be approximated in terms of N_{GL} values of sectional deformations ($\varepsilon_j = \boldsymbol{\varepsilon}\left(\xi_j\right)$ and $\kappa_j = \boldsymbol{\kappa}\left(\xi_j\right)$) as:

$$\varepsilon(x)=\sum_{j=1}^{N_{GL}} l_j(\xi)\varepsilon_j \quad \text{and} \quad \kappa(x)=\sum_{j=1}^{N_{GL}} l_j(\xi)\kappa_j \tag{31}$$

where $l_i(\xi)$ represents the Lagrange polynomial defined as:

$$l_j(\xi)=\frac{\prod_{i=1,i\neq j}^{N_{GL}}(\xi-\xi_i)}{\prod_{i=1,i\neq j}^{N_{GL}}(\xi_j-\xi_i)} \tag{32}$$

and has the following property:

$$l_j(\xi_i)=\delta_{ij} \tag{33}$$

Based on Eqs. (30) and (31), the axial-displacement $u(x)$ and vertical-displacement $v(x)$ fields can be recovered as:

$$\begin{aligned} u(x)&=L\left(\int\sum_{j=1}^{N_{GL}} l_j(\xi)\varepsilon_j d\xi+c_1\right)\\ v(x)&=L\left(\int\sum_{j=1}^{N_{GL}} l_j(\xi)\kappa_j d\xi+c_2\xi+c_3\right)\end{aligned} \tag{34}$$

where c_1, c_2, and c_3 are constants of integration and can be determined by imposing geometric boundary conditions. It is noted that the displacement recovery procedure employed herein is based on sectional deformations ($\varepsilon_j=\boldsymbol{\varepsilon}(\xi_j)$ and $\kappa_j=\boldsymbol{\kappa}(\xi_j)$) automatically computed during the element state determination. Therefore, this deformation-based displacement recovery procedure is well suited and natural to the employed element state determination. However, it must kept in mind that a nonphysical wriggling displacement profile may be obtained when excessive integration points are employed.

6. Numerical Examples

In this study, three numerical examples are employed to assess the accuracy and demonstrate the application and effectiveness of the proposed nonlocal frame model. The first example shows the model capability to eliminate the "*constant-force*" paradoxical responses inherent to the Eringen's nonlocal frame model and the simplified strain-gradient frame model; the second presents and

characterizes the essence of the material small-scale effect on global and local responses of a propped cantilever nanobeam; the third investigates the material small-scale effect on the tensile response of an auxetic metamaterial. It is worth emphasizing that every frame member in all examples is represented only by a single proposed frame element, thus requiring no finite-element discretization. Forty Gauss-Lobatto integration points are used for all numerical integrations in the element state determination and result in satisfactory numerical results especially for a small value of the nonlocal characteristic length l_c.

6.1 Example I: Paradox-Free Responses

An aluminum cantilever under different types of end loadings shown in Fig. 5 is utilized to present the ability of the proposed stress-driven nonlocal frame model to remedy the paradoxical responses associated with constant axial force (Fig. 5a), constant bending moment (Fig. 5b), and constant shear force (Fig. 5c). The beam length L is 20 *nm* and the beam-section shape is square with a dimension h of 1.67 *nm*, thus $A = 2.79\ nm^2$ and $I = 648.16\times10^{-3}\ nm^4$. The elastic modulus E_{xx} of aluminum is 68.5 *GPa* as provided by Oskouie et al. [58] and the material length-scale parameter $l_c = 5\ nm$ is selected to represent the material small-scale effect. Four different frame models based on various constitutive relations are employed and assessed. The first is the local (classical) frame model; the second is the Eringen nonlocal frame model of Limkatanyu et al. [34] and Limkatanyu et al. [37]; the third is the simplified strain-gradient frame model of Sae-Long et al. [52] and Sae-Long et al. [53]; and the fourth is the stress-driven nonlocal frame model proposed in this study. In addition, the analytical responses obtained with the differential form of the stress-driven nonlocal bar and beam models as given by Barretta et al. [59] and Romano and Barretta [31] are presented as "*benchmark*" responses to verify the validity of the proposed flexibility-based stress-driven nonlocal frame model.

6.1.1 Constant axial-force state

Under an axial force at its end ($P_{x0} = 50\ nN$

-gradient frame model are identical to that obtained with the local (classical) frame

simplified strain-gradient model [52] can capture the material small-scale effect. This peculiar observation is associated with the paradox inherent to the Eringen nonlocal constitutive model and has been extensively discussed in the literature [46, 52]. Employment of the simplified strain-gradient model leads to a well-posed structural-mechanics problem [54] and succeeds in remedying the famous paradoxical response of a cantilever beam under an end concentrated load [53] but fails to capture the material small-scale effect under the constant axial-force state. This failure is associated with the fact that the simplified strain-gradient model employed by Sae-Long et al. [52] can only consider the axial-strain gradient ($\partial\varepsilon/\partial x$) along the length. Nonetheless, under constant axial-force state, there is no axial-strain gradient ($\partial\varepsilon/\partial x = 0$) along the length, thus overlooking the material small-scale effect. For the stress-driven nonlocal integral model adopted herein, the material small-scale effect is considered through the convolution integral of Eq. (1) and leads to a stiffer displacement response. This stiffening system response is in good agreement with both experimental and analytical results reported by several researchers [14-16]. Fig. 6 also shows that the axial displacement profile obtained with the proposed nonlocal frame model can resemble the benchmark result, thus confirming the accuracy of the proposed nonlocal frame model.

Fig. 7 shows and compares the axial-force and axial-strain distributions associated with all frame models. Clearly, the axial-force and axial-strain distributions obtained with the proposed nonlocal frame model can resemble the benchmark responses, thus confirming the model validity. Fig. 7a indicates that all obtained axial-force distributions are identical regardless of the selected section constitutive model. This observation stems from a statically determinate nature of the system and has been noticed by several researchers [52-53]. Contrastingly, the axial-strain distribution obtained from the proposed stress-driven nonlocal frame model is different from those obtained from the other three frame models as shown in Fig. 7b. Accounting for the material small-scale effect via the stress-driven nonlocal model drastically alters the distribution nature of the axial strain along the length.

6.1.2 Constant bending-moment state

Under an end moment ($M_0 = 1.0\, nN - nm$), the cantilever of Fig. 5b is under a constant bending-moment state (pure-bending state). Fig. 8 superimposes and compares the vertical displacement distributions of this cantilever for all frame models. Similar to the observation from the

constant axial-force state, only the stress-driven nonlocal frame model is able to represent the material small-scale effect under the pure-bending state. As a result, the vertical-displacement distributions obtained with the Eringen nonlocal frame model and the simplified strain-gradient frame model are the same as that obtained with the local (classical) frame model. The implication of this observation is that under the pure-bending state, the material small-scale effect cannot be represented by either the Eringen nonlocal differential model [37] or the simplified strain-gradient model [53] but can only be detected by the stress-driven nonlocal model [31]. This bizarre observation is regarded as a paradox and its cause is the same as the one diagnosed for the aforementioned constant axial-force state. When compared to the benchmark response, the validity of the proposed nonlocal frame model is justified. The system-stiffness enhancement associated with the material small-scale effect can clearly be noticed in Fig. 8 and is in good agreement with both experimental and analytical evidences reported by several researchers [14-16].

The bending-moment and bending-curvature distributions obtained with all frame models are superimposed and compared in Fig. 9. Obviously, the bending-moment and bending-curvature distributions obtained with the proposed nonlocal frame model can resemble the benchmark responses. Due to a statically determinate nature of the system, all obtained bending-moment distributions shown in Fig. 9a are identical since they are merely governed by the equilibrium requirement. In accordance with the vertical-displacement distributions of Fig. 8, Fig. 9b indicates that the bending-curvature distribution obtained from the proposed stress-driven nonlocal frame model is distinct from those obtained from the other three frame models, thus confirming the ability of the proposed stress-driven nonlocal frame model to represent the material small-scale effect under the pure-bending state. It is worth observing that the bending-moment and bending-curvature distributions of Fig. 9 are similar to the axial-force and axial-strain distributions of Fig. 7. This observation stems from the fact that the section constitutive relations of Eqs. (1) and (2) are both subjected to constant section forces (constant axial force and constant bending moment). Therefore, the resulting axial-strain and bending-curvature distributions are alike. In other words, the problem associated with the constant axial-force state is identical to that associated with the constant bending-moment state.

6.1.3 Constant shear-force state

Under a vertical force at its end ($P_{y0} = 0.1\,nN$), the cantilever of Fig. 5c is under a constant shear-force state, thus resulting in a linear variation of bending moment. All obtained vertical-displacement distributions of this cantilever are plotted and compared in Fig. 10. Obviously, the vertical-displacement distributions obtained from the local frame model and the Eringen nonlocal frame model are identical while the vertical-displacement distributions obtained from the simplified strain-gradient frame model and the proposed stress-driven nonlocal frame model are different and stiffer than their local counterparts. The failure of the Eringen nonlocal frame model to represent the material small-scale effect for this particular case is the famous paradoxical phenomenon [43] and had been noticed and diagnosed by several researchers [31, 45-47]. In a rigorous mathematical manner, Romano et al. [47] proves that adoption of the Eringen nonlocal constitutive model leads to an ill-posed structural-mechanics problem, thus admitting no solution. Unlike constant axial-force and bending-moment states, accounting for the axial-strain gradient ($\partial\varepsilon / \partial x$) along the length renders the simplified strain-gradient frame model able to describe the material small-scale effect under constant shear-force state (linear bending-moment distribution). As shown in Fig. 10, the vertical-displacement response associated with the proposed stress-driven nonlocal frame model is stiffer than that associated with the simplified strain-gradient frame model. A similar observation is noticed by Oskouie et al. [89]. When compared to the benchmark response, the validity of the proposed nonlocal frame model is confirmed.

Fig. 11 plots and compares the bending-moment and bending-curvature distributions obtained with all frame models. Obviously, the bending-moment and bending-curvature distributions associated with the proposed nonlocal frame model can match the benchmark responses. All obtained bending-moment distributions shown in Fig. 11a are identical due to a statically determinate nature of the system. In accordance with the vertical-displacement distributions of Fig. 10, both strain gradient and stress-driven nonlocality drastically alter the distribution nature of the bending-curvature response as shown in Fig. 11b.

6.2 Example II: Propped-Cantilever Nanobeam with Uniformly Distributed Load

Fig. 12 shows a propped-cantilever iron nanobeam subjected to a uniformly distributed load with a magnitude of $w_{y0} = 20\,nN/nm$

$I = 16.67 \times 10^6\ nm^4$. As given by Lim

and He [90] and Mahmoud et al. [91], the elastic modulus E_{xx} of the iron nanobeam is 56.25 *GPa*. The material length-scale parameter l_c is 200 *nm* as used by Yang and Lim [92]. To investigate the material small-scale effect on this propped cantilever, both global and local bending responses obtained with the simplified strain-gradient frame model of Sae-Long et al. [52-53] and the proposed stress-driven nonlocal frame model are compared to those obtained with the local frame model.

Fig. 13 plots and compares all obtained vertical-displacement responses. The simplified strain-gradient frame model and the proposed stress-driven nonlocal frame model consistently result in stiffer displacement responses when compared to the local frame model. However, the stiffening phenomenon associated with the material nonlocality is more pronounced than that associated with the material strain gradient. It is interesting to observe that all frame models yield the same location of maximum displacement at 600 *nm* from the clamped end. Therefore, the maximum-displacement location is only dictated by beam end geometric constraints. When compared to the benchmark response, Fig. 13 also confirms the validity of the proposed nonlocal frame model.

Fig. 14 plots and compares the bending-moment and bending-curvature distributions obtained with all frame models. It is clear that the bending-moment and bending-curvature distributions associated with the proposed nonlocal frame model can match the benchmark responses. Unlike the cantilever of Example I, Fig. 14a shows that different section constitutive models result in distinct bending-moment distributions due to a statically indeterminate nature of the system. However, the distribution characteristic of the bending moment is marginally affected by the presence of the material small-scale effect (either the material nonlocality or the material strain gradient). The maximum values of positive and negative bending moment are more or less the same for all frame models. Contrastingly, Fig. 14b shows that the material small-scale effect drastically alters the distribution nature of the bending curvature and reduces the maximum values of positive and negative bending curvature when compared to those obtained with the local frame model. With the proposed stress-driven nonlocal frame model and the simplified strain-gradient frame model, the obtained bending-curvature distributions tend to be spread more gradually along the beam length. With the presence of the material small-scale effect, the system stiffness is increased as shown in Fig. 13 while the maximum value of bending curvature (positive and negative) is decreased as shown in Fig. 14b. The

combination of these two consequences yields the reason why the distribution characteristic of the bending moment shown in Fig. 14a is marginally affected by the material small-scale effect.

6.3 Example III: Small-Scale Effect on Tensile Response of an Auxetic Metamaterial

In recent years, researchers worldwide have paid considerable attention to studies of auxetic metamaterials due to their wide spectrum of novel applications and unusual mechanical properties [9-11]. Among these unusual mechanical properties, a negative Poisson's ratio is the most prominent and is related to the topology of their micro/nano architecture [9-11]. This example investigates the material small-scale effect on tensile response of an auxetic metamaterial. Fig 15 shows a two-dimensional quadrangular strip subjected to a tensile loading at its right end. This quadrangular strip is made of an auxetic metamaterial formed by re-entrant bow-tie cells consisted of titanium struts [54]. The elastic modulus E_{xx} of the titanium strut is 110 *GPa*. The strut-section shape is square with a dimension *h* of 1.0 *nm*, thus $A = 1\ nm^2$ and $I = 83.33\times10^{-3}\ nm^4$. Each strut in re-entrant bow-tie cells is modeled by a single nonlocal frame element proposed herein. As a result, 35 nonlocal frame elements are employed to represent the quadrangular strip. To investigate the material small-scale effect on tensile response of the quadrangular strip, the nonlocal characteristic length l_c is varied through the normalized nonlocal parameter $\overline{\lambda} = l_c / L$ ranging from 0 to 0.5.

Following the variables defined in Fig. 15, strains in axial and lateral directions (ε_{xx} and ε_{yy}) and Poisson's ratio ν are computed as:

$$\varepsilon_{xx} = \frac{\Delta_x}{L_x};\ \varepsilon_{yy} = \frac{2\Delta_y}{L_y};\ \text{and}\ \nu = -\frac{\varepsilon_{yy}}{\varepsilon_{xx}} \tag{35}$$

where Δ_x and Δ_y represent axial and lateral deformations of the quadrangular strip, respectively; and L_x and L_y defines the length and width of the quadrangular strip, respectively. The normalized axial stiffness $\overline{K}$ is defined as:

$$\overline{K} = \frac{\Delta_x^L}{\Delta_x^{NL}} \tag{36}$$

where Δ_x^{NL} defines the axial deformation obtained with the proposed stress-driven nonlocal frame model while Δ_x^{L} defines the axial deformation obtained with the local frame model under the same imposed end force P_{x0}.

Figs. 16 and 17 present the material small-scale effect on the normalized axial stiffness $\overline{K}$ and Poisson's ratio ν, respectively. As shown in Fig. 16, the normalized axial stiffness $\overline{K}$ increases with increasing normalized nonlocal parameter $\overline{\lambda}$, thus confirming the essence of the stiffening phenomenon for auxetic metamaterials at nanoscale. Fig. 17 shows that the magnitude of negative Poisson's ratio ν decreases with increasing normalized nonlocal parameter $\overline{\lambda}$. This observation infers that the counterintuitive response of auxetic metamaterials becomes less pronounced when the material small-scale effect is considered.

7. Summary and Conclusions

In this paper, an efficient frame element is developed for analyses of nano-sized frames. The stress-driven nonlocal integral model is adopted to represent the material small-scale effect inherent to nano-sized frames. For the present interest of frame analyses, this nonlocal constitutive model affirms that the deformation at any section is induced by its corresponding forces at all sections along the frame length via a convolution integral statement. The flexibility-based finite element formulation is employed to construct the proposed nonlocal frame element and is well suited to the stress-driven nonlocal integral model. With this type of finite element formulation, equilibrated force interpolation functions are used to express the element sectional forces in terms of the element forces, thus resulting in the "*exact*" element flexibility equation. The "*exact*" element stiffness equation is finally obtained based on the exact element flexibility equation using the rigid-body-mode transformation, thus rendering the "*one-element-per-member*" modeling approach applicable. To the best of authors' knowledge, the proposed frame element is the first flexibility-based nonlocal frame model present in the research community and takes full advantage of "*exact*" force interpolation functions in the model formulation. The element state determination process as well as the displacement recovery procedure are also presented. Three numerical examples are employed to assess validity and effectiveness as well as to characterize and investigate the small-scale effect on both global and local responses of nano-sized frames.

The first example considers an aluminum cantilever under three internal force states, namely: constant axial force, constant bending moment, and constant shear force. Only the proposed nonlocal frame model can capture the material small-scale effect on displacement responses for all internal force states while the simplified strain-gradient frame model is capable of representing such an effect only for constant shear-force state. The widely used Eringen nonlocal frame model presents no material small-scale effect for all internal force states. As a result, the proposed stress-driven nonlocal frame model is "*paradox free*". When material small-scale effect is considered, the displacement response predicted by the proposed nonlocal frame model is stiffer than that predicted by the local frame model. This system-stiffness enhancement is in good agreement with both experimental evidences and theoretical results reported in literature.

The second example focuses on a propped-cantilever iron nanobeam under uniformly distributed load. Both the stress-driven nonlocal frame model and the simplified strain-gradient model predict stiffer displacement responses when compared to the local frame model. However, the stiffening phenomenon associated with the material strain gradient is less pronounced than that associated with the material nonlocality. Different bending-moment distributions are obtained with different constitutive models due to a statically indeterminate nature of the system but their distribution characteristics are marginally affected with the presence of the material small-scale effect. The maximum values of positive and negative bending moment are approximately the same for all frame models. In opposition, the material small-scale effect drastically alters the distribution nature of the bending curvature. With the proposed stress-driven nonlocal frame model and the simplified strain-gradient frame model, the obtained bending-curvature distributions tend to be spread more gradually along the beam length and their maximum values of positive and negative bending curvature are reduced.

The third example studies tensile response of an auxetic metamaterial quadrangular strip. Due to the topology of its micro/nano architecture, this auxetic metamaterial quadrangular strip possesses a negative Poisson's ratio. With increasing nonlocal parameter, the axial stiffness of the quadrangular strip increases while the magnitude of negative Poisson's ratio ν decreases, thus emphasizing the essence of the material small-scale effect on the auxetic metamaterials at nanoscale.

One next step forward in this research direction is to include material and geometric nonlinearities into the nonlocal frame model and is the extension to the space frame. In addition,

accounting for the surface effect would yield a more rational nanoframe model and is worth pursuing in future research work. It is expected that the proposed nanoframe model will be useful to scientists and engineers conducting research in the area of nanoscience and nanoengineering.

Acknowledgments

This study was supported by the TRF Senior Research Scholar under Grant RTA 6280012. Any opinions expressed in this paper are those of the authors and do not reflect the views of the sponsoring agencies. Special thanks go to a senior lecturer Mr. Wiwat Sutiwipakorn for reviewing and correcting the English of this paper.

Competing interests

The authors declare that they have no competing interests

Authors' contributions

Suchart Limkatanyu plays a role in formulating the numerical model, interpreting the numerical results, and partially writing the manuscript; **Worathep Sae-Long** plays a role in implementing the numerical model, interpreting the numerical results and partially writing the manuscript; **Hamid M. Sedighi** plays a role in advising the application of the stress-driven nonlocal integral model and interpreting the numerical results; **Jaroon Rungamornrat** plays a role in in advising the model implementation and interpreting the numerical results; **Piti Sukontasukkul** plays a role in suggesting the modeling approach of an auxetic metamaterial; **Hexin Zhang** plays a role in revising the manuscript and proving the general comment; and **Prinya Chindaprasirt** plays a role in initiating the model application on an auxetic metamaterial.

Conflict of interest

The authors declare that they have no conflict of interest

References

1. Meyer G, Amer NM (1990) Simultaneous measurement of lateral and normal forces with an optical-beam-deflection atomic force microscope. Appl Phys Lett 57:2089. https://doi.org/10.1063/1.103950
2. Sader JE, Chon JWM, Mulvaney P (1999) Calibration of rectangular atomic force microscope cantilevers. Rev Sci Instrum 70:3967. https://doi.org/10.1063/1.1150021
3. Dantas WG, Gusso A (2018) Analysis of the chaotic dynamics of MEMS/NEMS doubly clamped beam resonators with two-sided electrodes. Int J Bifurcation Chaos 28(10):1850122. https://doi.org/10.1142/S0218127418501225
4. Dilena M, Dell'Oste MF, Fernández-Sáez J, Morassi A, Zaera R (2020) Hearing distributed mass in nanobeam resonators. Int J Solids Struct 193-194: 568-592. https://doi.org/10.1016/j.ijsolstr.2020.02.025
5. Dastjerdi S, Akgöz B, Civalek Ö (2020) On the effect of viscoelasticity on behavior of gyroscopes. Int J Eng Sci 149:103236. https://doi.org/10.1016/j.ijengsci.2020.103236
6. Larkin K, Ghommem M, Serrano M, Abdelkefi A (2021) A review on vibrating beam-based micro/nano-gyroscopes. Microsyst Technol. https://doi.org/10.1007/s00542-020-05191-z
7. Xiao W, Huan J, Liu G, Shi H, Dong S (2013) A digitally linear piezoelectric bimorph actuator in open-loop mode. Appl Phys Lett 102:123503. https://doi.org/10.1063/1.4798589
8. Longo G, Alonso-Sarduy L, Rio LM et al (2013) Rapid detection of bacterial resistance to antibiotics using AFM cantilevers as nanomechanical sensors. Nat Nanotechnol 8:522-526. https://doi.org/10.1038/nnano.2013.120
9. Valente J, Plum E, Youngs IJ, Zheludev NI (2016) Nano- and micro-auxetic plasmonic materials. Adv Mater 28(26):5176-5180. https://doi.org/10.1002/adma.201600088
10. Spanos I, Vangelatos Z, Grigoropoulos C, Farsari M (2021) Design and characterization of microscale auxetic and anisotropic structures fabricated by multiphoton lithography. Nanomater 11(2):446. https://doi.org/10.3390/nano11020446
11. Hajmohammad MH, Nouri AH, Zarei MS, Kolahchi R (2019) A new numerical approach and visco-refined zigzag theory for blast analysis of auxetic honeycomb plates integrated by multiphase nanocomposite facesheets in hygrothermal environment. Eng Comput 35:1141-1157. https://doi.org/10.1007/s00366-018-0655-x
12. Xie B, Liu Y, Ding Y, Zheng Q, Xu Z (2011) Mechanics of carbon nanotube networks: microstructural evolution and optimal design. Soft Matter 7(21):10039. https://doi.org/10.1039/C1SM06034A
13. Zhang C, Akbarzadeh A, Kang W, Wang J, Mirabolghasemi A (2018) Nano-architected metamaterials: Carbon nanotube-based nanotrusses. Carbon 131:38-46. https://doi.org/10.1016/j.carbon.2018.01.082
14. Fleck NA, Muller GM, Ashby MF, Hutchinson JW (1994) Strain gradient plasticity: Theory and experiment. Acta Metall Mater 42(2):475-487. https://doi.org/10.1016/0956-7151(94)90502-9
15. Poole WJ, Ashby MF, Fleck NA (1996) Micro-hardness of annealed and work-hardened copper polycrystals. Scr Mater 34(4):559-564. https://doi.org/10.1016/1359-6462(95)00524-2
16. Lam DCC, Yang F, Chong ACM, Wang J, Tong P (2003) Experiments and theory in strain gradient elasticity. J Mech Phys Solids 51(8):1477-1508. https://doi.org/10.1016/S0022-5096(03)00053-X
17. Zhang CL, Shen HS (2008) Predicting the elastic properties of double-walled carbon nanotubes by molecular dynamics simulation. J Phys D: Appl Phys 41(5):055404. https://doi.org/10.1088/0022-3727/41/5/055404
18. Madani SH, Sabour MH, Fadaee M (2018) Molecular dynamics simulation of vibrational behavior of annular graphene sheet: Identification of nonlocal parameter. J Mol Graphics Modell 79:264-272. https://doi.org/10.1016/j.jmgm.2017.11.008
19. Zhong L, Yili Z, Buyun W, Hao C, Xiren C, Zhengcan H (2018) DFT study on Al-doped defective graphene towards adsorption of elemental mercury. Appl Surf Sci 427(A):547-553. https://doi.org/10.1016/j.apsusc.2017.07.293
20. Ghavanloo E, Fazelzadeh SA, Marotti de Sciarra F (2021) Size-dependent continuum mechanics approaches. Springer International Publishing. https://doi.org/10.1007/978-3-030-63050-8
21. Shahabodini A, Gholami Y, Ansari R, Rouhi H (2019) Vibration analysis of graphene sheets resting on Winkler/Pasternak foundation: A multiscale approach. Eur Phys J Plus 134:510. https://doi.org/10.1140/epjp/i2019-12856-x
22. Altan BS, Aifantis EC (1997) On some aspects in the special theory of gradient elasticity. J Mech Behav Mater 8(3):231-282. https://doi.org/10.1515/JMBM.1997.8.3.231

23. Fu G, Zhou S, Qi L (2019) A size-dependent Bernoulli-Euler beam model based on strain gradient elasticity theory incorporating surface effects. ZAMM 99(6):e201800048. https://doi.org/10.1002/zamm.201800048
24. Zhang GY, Gao XL (2020) A new Bernoulli–Euler beam model based on a reformulated strain gradient elasticity theory. Math Mech Solids 25:630-643. https://doi.org/10.1177/1081286519886003
25. Mindlin RD, Tiersten HF (1962) Effects of couple-stresses in linear elasticity. Arch Ration Mech Anal 11:415-448. https://doi.org/10.1007/BF00253946
26. Liu H, Shen SX, Oslub K, Habibi M, Safarpour H (2021) Amplitude motion and frequency simulation of a composite viscoelastic microsystem within modified couple stress elasticity. Eng Comput. https://doi.org/10.1007/s00366-021-01316-8
27. Ma HM, Gao XL, Reddy JN (2008) A microstructure-dependent Timoshenko beam model based on a modified couple stress theory. J Mech Phys Solids 56(12):3379-3391. https://doi.org/10.1016/j.jmps.2008.09.007
28. Jung WY, Han SC (2015) Static and eigenvalue problems of Sigmoid Functionally Graded Materials (S-FGM) micro-scale plates using the modified couple stress theory. Appl Math Modell 39(12):3506-3524. https://doi.org/10.1016/j.apm.2014.11.056
29. Eringen AC (1972) Nonlocal polar elastic continua. Int J Eng Sci 10(1):1-16. https://doi.org/10.1016/0020-7225(72)90070-5
30. Faghidian SA, Mohammad-Sedighi H (2020) Dynamics of nonlocal thick nano-bars. Eng Comput. https://doi.org/10.1007/s00366-020-01216-3
31. Romano G, Barretta R (2017) Nonlocal elasticity in nanobeams: the stress-driven integral model. Int J Eng Sci 115:14-27. https://doi.org/10.1016/j.ijengsci.2017.03.002
32. Apuzzo A, Barretta R, Fabbrocino F, Faghidian SA, Luciano R, Marotti de Sciarra F (2019) Axial and torsional free vibrations of elastic nano-beams by stress-driven two-phase elasticity. J Appl Comput Mech 5(2):402-413. https://doi.org/10.22055/jacm.2018.26552.1338
33. Vaccaro MS, Pinnola FP, Marotti de Sciarra F, Barretta R (2021) Elastostatics of Bernoulli-Euler beams resting on displacement-driven nonlocal foundation. Nanomater 11(3):573. https://doi.org/ 10.3390/nano11030573
34. Limkatanyu S, Damrongwiriyanupap N, Prachasaree W, Sae-Long W (2013) Modeling of axially loaded nanowires embedded in elastic substrate media with inclusion of nonlocal and surface effects. J Nanomater:635428. https://doi.org/10.1155/2013/635428
35. Hamed MA, Mohamed NA, Eltaher MA (2020) Stability buckling and bending of nanobeams including cutouts. Eng Comput. https://doi.org/10.1007/s00366-020-01063-2
36. Juntarasaid C, Pulngern T, Chucheepsakul S (2012) Bending and buckling of nanowires including the effects of surface stress and nonlocal elasticity. Physica E 46:68-76. https://doi.org/10.1016/j.physe.2012.08.005
37. Limkatanyu S, Sae-Long W, Horpibulsuk S, Prachasaree W, Damrongwiriyanupap N (2018) Flexural responses of nanobeams with coupled effects of nonlocality and surface energy. ZAMM 98(10):1771-1793. https://doi.org/10.1002/zamm.201700311
38. Civalek Ö, Demir Ç (2011) Bending analysis of microtubules using nonlocal Euler–Bernoulli beam theory. Appl Math Modell 35(5):2053-2067. https://doi.org/10.1016/j.apm.2010.11.004
39. Demir Ç, Mercan K, Numanoglu HM, Civalek Ö (2018) Bending response of nanobeams resting on elastic foundation. J Appl Comput Mech 4(2):105-114. https://doi.org/10.22055/jacm.2017.22594.1137
40. Eltaher MA, Khater ME, Emam SA (2016) A review on nonlocal elastic models for bending, buckling, vibrations, and wave propagation of nanoscale beams. Appl Math Modell 40(5-6):4109-4128. https://doi.org/10.1016/j.apm.2015.11.026
41. Tran VK, Pham QH, Nguyen-Thoi T (2020) A finite element formulation using four-unknown incorporating nonlocal theory for bending and free vibration analysis of functionally graded nanoplates resting on elastic medium foundations. Eng Comput. https://doi.org/10.1007/s00366-020-01107-7
42. Hadji L, Avcar M, Civalek Ö (2021) An analytical solution for the free vibration of FG nanoplates. J Braz Soc Mech Sci Eng 43:418. https://doi.org/10.1007/s40430-021-03134-x
43. Peddieson J, Buchanan GR, McNitt RP (2003) Application of nonlocal continuum models to nanotechnology. Int J Eng Sci 41(3-5):305-312. https://doi.org/10.1016/S0020-7225(02)00210-0
44. Wang CM, Kitipornchai S, Lim CW, Eisenberger M (2008) Beam bending solutions based on nonlocal Timoshenko beam theory. J Eng Mech 134(6):475-481. https://doi.org/10.1061/(ASCE)0733-9399(2008)134:6(475)

45. Challamel N, Wang CM (2008) The small length scale effect for a non-local cantilever beam: a paradox solved. Nanotechnol 19(34):345703. https://doi.org/10.1088/0957-4484/19/34/345703
46. Benvenuti E, Simone A (2013) One-dimensional nonlocal and gradient elasticity: Closed-form solution and size effect. Mech Res Commun 48:46-51. https://doi.org/10.1016/j.mechrescom.2012.12.001
47. Romano G, Barretta R, Diaco M, Marotti de Sciarra F (2017) Constitutive boundary conditions and paradoxes in nonlocal elastic nanobeams. Int J Mech Sci 121:151-156. https://doi.org/10.1016/j.ijmecsci.2016.10.036
48. Vaccaro MS, Pinnola FP, Marotti de Sciarra F, Barretta R (2021) Limit behaviour of Eringen's two-phase elastic beams. Eur J Mech A Solids 89:104315. https://doi.org/10.1016/j.euromechsol.2021.104315
49. Barretta R, Marotti de Sciarra F (2013) A nonlocal model for carbon nanotubes under axial loads. Adv Mater Sci Eng:360935. https://doi.org/10.1155/2013/360935
50. Akgöz B, Civalek Ö (2015) A microstructure-dependent sinusoidal plate model based on the strain gradient elasticity theory. Acta Mech 226:2277-2294. https://doi.org/10.1007/s00707-015-1308-4
51. Barretta R, Faghidian SA, Marotti de Sciarra F (2019) Aifantis versus Lam strain gradient models of Bishop elastic rods. Acta Mech 230:2799-2812. https://doi.org/10.1007/s00707-019-02431-w
52. Sae-Long W, Limkatanyu S, Prachasaree W, Rungamornrat J, Sukontasukkul P (2020) A thermodynamics-based nonlocal bar-elastic substrate model with inclusion of surface-energy effect. J Nanomater:8276745. https://doi.org/10.1155/2020/8276745
53. Sae-Long W, Limkatanyu S, Rungamornrat J, Prachasaree W, Sukontasukkul P, Sedighi HM (2021) A rational beam-elastic substrate model with incorporation of beam-bulk nonlocality and surface-free energy. Eur Phys J Plus 136:80. https://doi.org/10.1140/epjp/s13360-020-00992-7
54. Niiranen J, Balobanov V, Kiendl J, Hosseini SB (2017) Variational formulations, model comparisons and numerical methods for Euler-Bernoulli micro- and nano-beam models. Math Mech Solids 24(1): 108128651773966. https://doi.org/10.1177/1081286517739669
55. Romano G, Barretta R (2017) Stress-driven versus strain-driven nonlocal integral model for elastic nano-beams. Composites, Part B 114:184-188. https://doi.org/10.1016/j.compositesb.2017.01.008
56. Apuzzo A, Barretta R, Luciano R, Marotti de Sciarra F, Penna R (2017) Free vibrations of Bernoulli-Euler nano-beams by the stress-driven nonlocal integral model. Composites, Part B 123:105-111. https://doi.org/10.1016/j.compositesb.2017.03.057
57. Vaccaro MS, Marotti de Sciarra F, Barretta R (2021) On the regularity of curvature fields in stress-driven nonlocal elastic beams. Acta Mech 232(7):2595-2603. https://doi.org/10.1007/s00707-021-02967-w
58. Oskouie MF, Ansari R, Rouhi H (2018) Bending of Euler–Bernoulli nanobeams based on the strain-driven and stress-driven nonlocal integral models: a numerical approach. Acta Mech Sin 34:871-882. https://doi.org/10.1007/s10409-018-0757-0
59. Barretta R, Faghidian SA, Luciano R (2019) Longitudinal vibrations of nano-rods by stress-driven integral elasticity. Mech Adv Mater Struct 26(15):1307-1315. https://doi.org/10.1080/15376494.2018.1432806
60. Yang X, Sahmani S, Safaei B (2021) Postbuckling analysis of hydrostatic pressurized FGM microsized shells including strain gradient and stress-driven nonlocal effects. Eng Comput 37:1549-1564. https://doi.org/10.1007/s00366-019-00901-2
61. Barretta R, Faghidian SA, Marotti de Sciarra F (2019) Stress-driven nonlocal integral elasticity for axisymmetric nano-plates. Int J Eng Sci 136:38-52. https://doi.org/10.1016/j.ijengsci.2019.01.003
62. Barretta R, Fabbrocino F, Luciano R, Marotti de Sciarra F, Ruta G (2020) Buckling loads of nano-beams in stress-driven nonlocal elasticity. Mech Adv Mater Struct 27(11):869-875. https://doi.org/10.1080/15376494.2018.1501523
63. Ouakad HM, Valipour A, Żur KK, Sedighi HM, Reddy JN (2020) On the nonlinear vibration and static deflection problems of actuated hybrid nanotubes based on the stress-driven nonlocal integral elasticity. Mech Mater 148:103532. https://doi.org/10.1016/j.mechmat.2020.103532
64. Bian PL, Qing H (2021) On bending consistency of Timoshenko beam using differential and integral nonlocal strain gradient models. ZAMM 101(8):e202000132. https://doi.org/10.1002/zamm.202000132

65. Moghtaderi SH, Faghidian SA, Asghari M (2020) Nonlinear vibrations of gradient and nonlocal elastic nano-bars. Mech Based Des Struct Mach. https://doi.org/10.1080/15397734.2020.1864640
66. Alotta G, Failla G, Zingales M (2014) Finite element method for a nonlocal Timoshenko beam model. Finite Elem Anal Des 89:77-92. https://doi.org/10.1016/j.finel.2014.05.011
67. Khodabakhshi P, Reddy JN (2015) A unified integro-differential nonlocal model. Int J Eng Sci 95:60-75. https://doi.org/10.1016/j.ijengsci.2015.06.006
68. Tuna M, Kirca M (2017) Bending, buckling and free vibration analysis of Euler-Bernoulli nanobeams using Eringen's nonlocal integral model via finite element method. Compos Struct 179:269-284. https://doi.org/10.1016/j.compstruct.2017.07.019
69. Norouzzadeh A, Ansari R (2017) Finite element analysis of nano-scale Timoshenko beams using the integral model of nonlocal elasticity. Physica E 88:194-200. https://doi.org/10.1016/j.physe.2017.01.006
70. Pinnola FP, Vaccaro MS, Barretta R, Marotti de Sciarra F (2022) Finite element method for stress-driven nonlocal beams. Eng Anal Boundary Elem 134:22-34. https://doi.org/10.1016/j.enganabound.2021.09.009
71. Rabczuk T, Ren H, Zhuang X (2019) A Nonlocal operator method for partial differential equations with application to electromagnetic waveguide problem. Comput, Mater Continua 59(1):31-55. https://doi.org/ 10.32604/cmc.2019.04567
72. Ren H, Zhuang X, Rabczuk T (2020) A higher order nonlocal operator method for solving partial differential equations. Comput Methods Appl Mech Eng 367:113132. https://doi.org/10.1016/j.cma.2020.113132
73. Ren H, Zhuang X, Oterkus E, Zhu H, Rabczuk T (2021) Nonlocal strong forms of thin plate, gradient elasticity, magneto-electro-elasticity and phase-field fracture by nonlocal operator method. Eng Comput. https://doi.org/10.1007/s00366-021-01502-8
74. Ren H, Zhuang X, Rabczuk T (2020) Nonlocal operator method with numerical integration for gradient solid. Comput Struct 233:106235. https://doi.org/10.1016/j.compstruc.2020.106235
75. Numanoğlu HM, Civalek Ö (2019) On the dynamics of small-sized structures. Int J Eng Sci 145:103164. https://doi.org/10.1016/j.ijengsci.2019.103164
76. Russillo AF, Failla G, Alotta G, Marotti de Sciarra F, Barretta R (2021) On the dynamics of nano-frames. Int J Eng Sci 160:103433. https://doi.org/10.1016/j.ijengsci.2020.103433
77. Syms RRA, Liu D, Ahmad MM (2017) Nanostructured 2D cellular materials in silicon by sidewall transfer lithography NEMS. J Micromech Microeng 27:075003.
78. Que L, Park J, Gianchandani YB (2001) Bent-beam electrothermal actuators-Part I: Single beam and cascaded devices. J Microelectromech Syst 10(2):247-254. https://doi.org/10.1109/84.925771
79. Hozhabrossadati SM, Challamel N, Rezaiee-Pajand M, Sani AA (2020) Free vibration of a nanogrid based on Eringen's stress gradient model. Mech Based Des Struct Mach. https://doi.org/10.1080/15397734.2020.1720720
80. Limkatanyu S, Spacone E (2002) Reinforced concrete frame element with bond interfaces. I: Displacement-based, force-based, and mixed formulations. J Struct Eng 128(3):346-355. https://doi.org/10.1061/(ASCE)0733-9445(2002)128:3(346)
81. Jafari V, Abyaneh MA, Vahdani SH, Rahimian M (2009) Improved displacement-field approximation for geometrical nonlinear flexibility-based planar curved element in state space. Mech Based Des Struct Mach 37(4):475-502. https://doi.org/10.1080/15397730903164094
82. Feng DC, Ren XD (2017) Enriched force-based frame element with evolutionary plastic hinge. J Struct Eng 143(10):06017005. https://doi.org/10.1061/(ASCE)ST.1943-541X.0001871
83. Feng DC, Wu G, Ning CL (2019) A regularized force-based Timoshenko fiber element including flexure-shear interaction for cyclic analysis of RC structures. Int J Mech Sci 160:59-74. https://doi.org/10.1016/j.ijmecsci.2019.06.011
84. Sae-Long W, Limkatanyu S, Hansapinyo C, Prachasaree W, Rungamornrat J, Kwon M (2021) Nonlinear flexibility-based beam element on Winkler-Pasternak foundation. Geomech Eng 24(4):371-388. https://doi.org/10.12989/gae.2021.24.4.371
85. Taylor RL (2000) FEAP: A finite element analysis program, User manual: version 7.3. Department of Civil and Environmental Engineering, University of California, Berkeley, California, USA.
86. Elias ZM (1986) Theory and methods of structural analysis. John Wiley & Sons, New York, USA.
87. Tonti E (1976) The reason for analogies between physical theories. Appl Math Modell 1(1):37-50. https://doi.org/10.1016/0307-904X(76)90023-8

88. Limkatanyu S, Spacone E (2002) Reinforced concrete frame element with bond interfaces. II: State determinations and numerical validation. J Struct Eng 128(3):356-364. https://doi.org/10.1061/(ASCE)0733-9445(2002)128:3(356)
89. Oskouie MF, Ansari R, Rouhi H (2018) Stress-driven nonlocal and strain gradient formulations of Timoshenko nanobeams. Eur Phys J Plus 133:336. https://doi.org/10.1140/epjp/i2018-12183-x
90. Lim CW, He LH (2004) Size-dependent nonlinear response of thin elastic films with nano-scale thickness. Int J Mech Sci 46(11):1715-1726. https://doi.org/10.1016/j.ijmecsci.2004.09.003
91. Mahmoud FF, Eltaher MA, Alshorbagy AE, Meletis EI (2012) Static analysis of nanobeams including surface effects by nonlocal finite element. J Mech Sci Technol 26:3555-3563. https://doi.org/10.1007/s12206-012-0871-z
92. Yang Y, Lim CW (2012) Non-classical stiffness strengthening size effects for free vibration of a nonlocal nanostructure. Int J Mech Sci 54(1):57-68. https://doi.org/10.1016/j.ijmecsci.2011.09.007

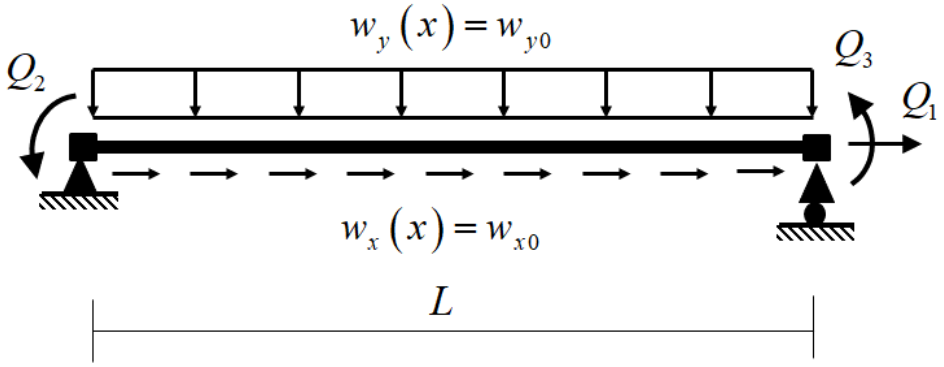

(a)

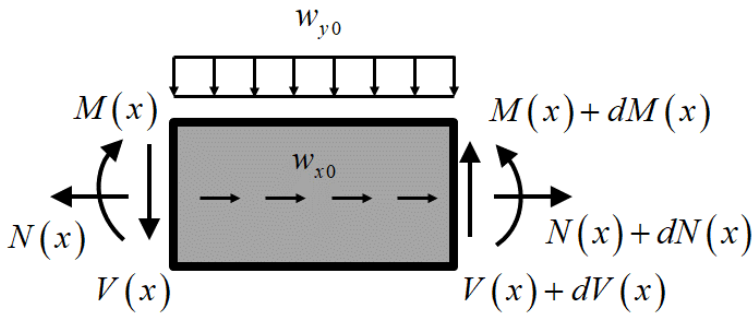

(b)

Fig. 1 (a) A nonlocal simply-supported frame under external loads; (b) A differential segment cut from the frame

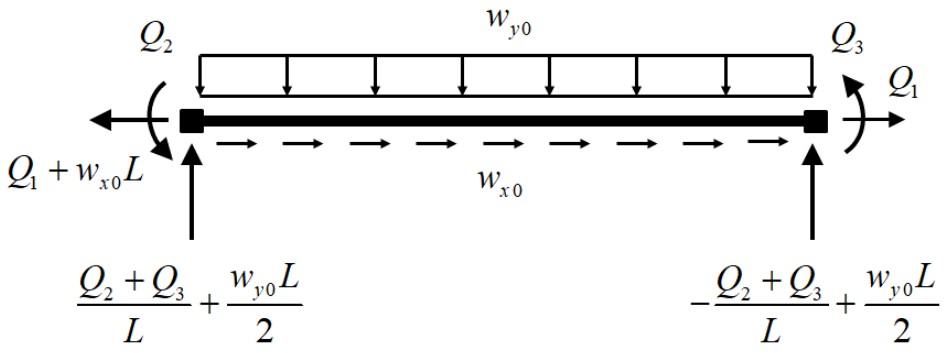

(a)

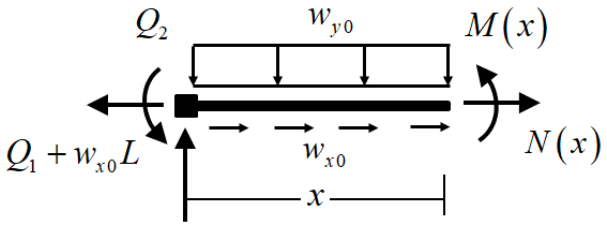

(b)

Fig. 2 (a) A nonlocal simply-supported frame of Figure 1 (a) with support reactions; (b) A cut segment from the frame

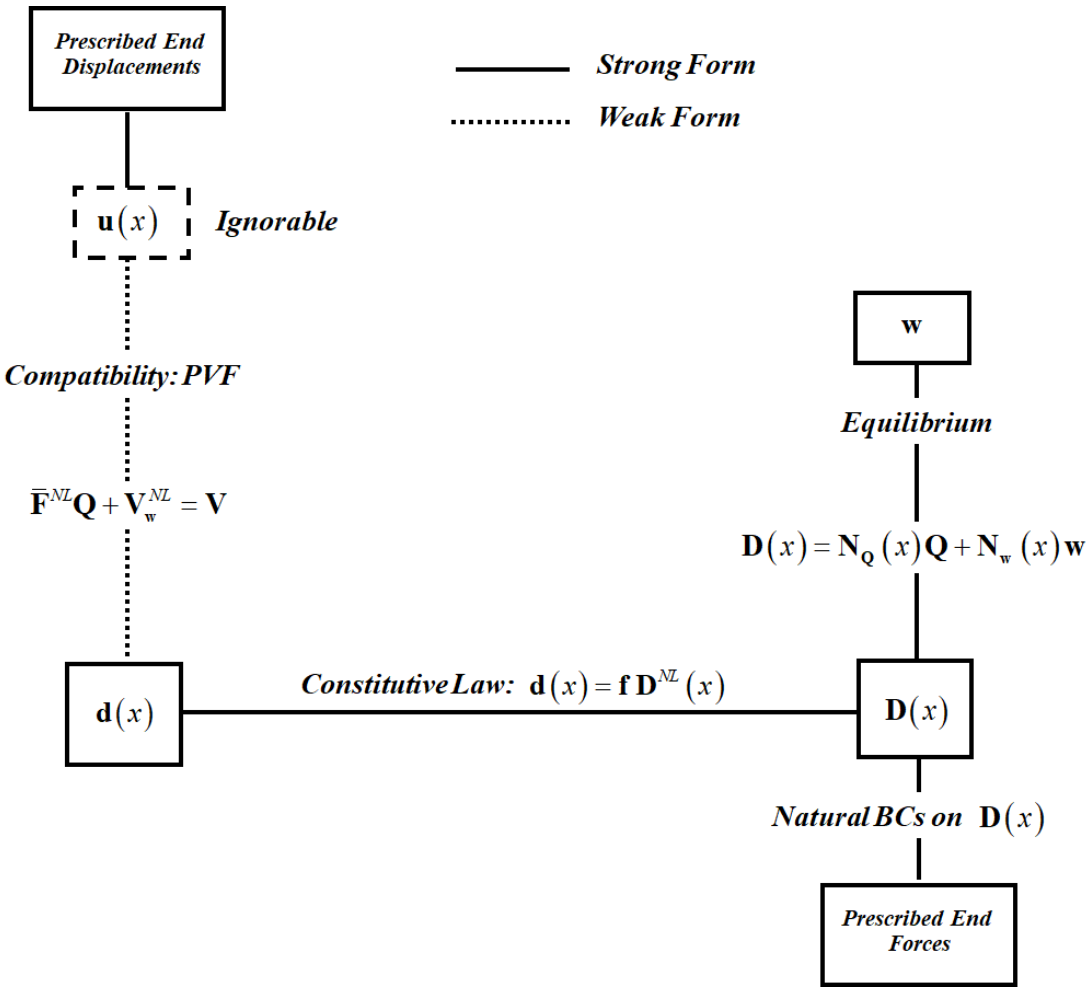

Fig. 3 Tonti's diagram for flexibility-based stress driven nonlocal frame element

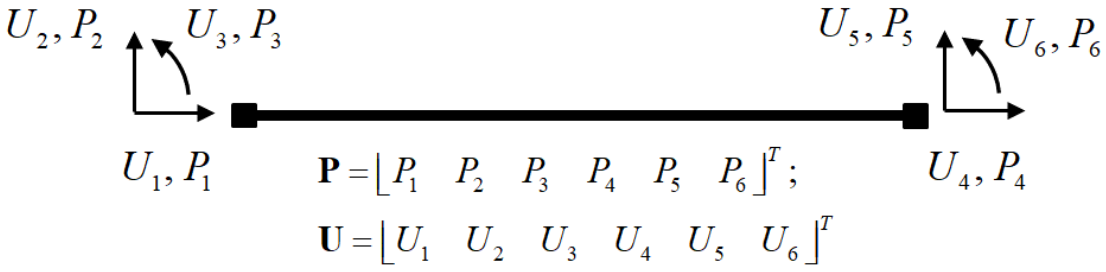

(a) System with Rigid-Body Modes (Complete System)

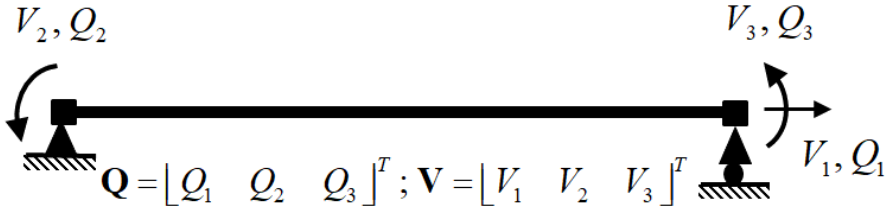

(b) System without Rigid-Body Modes (Basic System)

Fig. 4 Element force and displacement degrees of freedom: (a) complete system; and (b) basic system

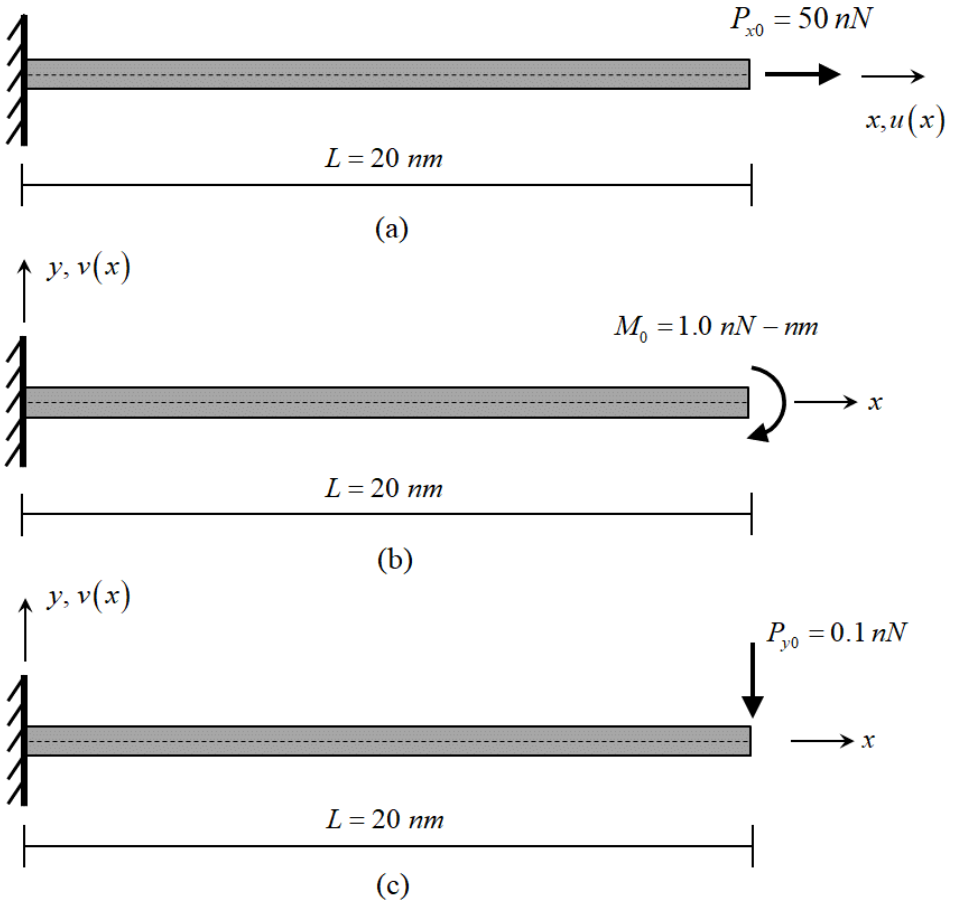

Fig. 5 Example I: aluminum cantilever subjected to different loading states: (a) constant axial force; (b) constant bending moment; (c) constant shear force

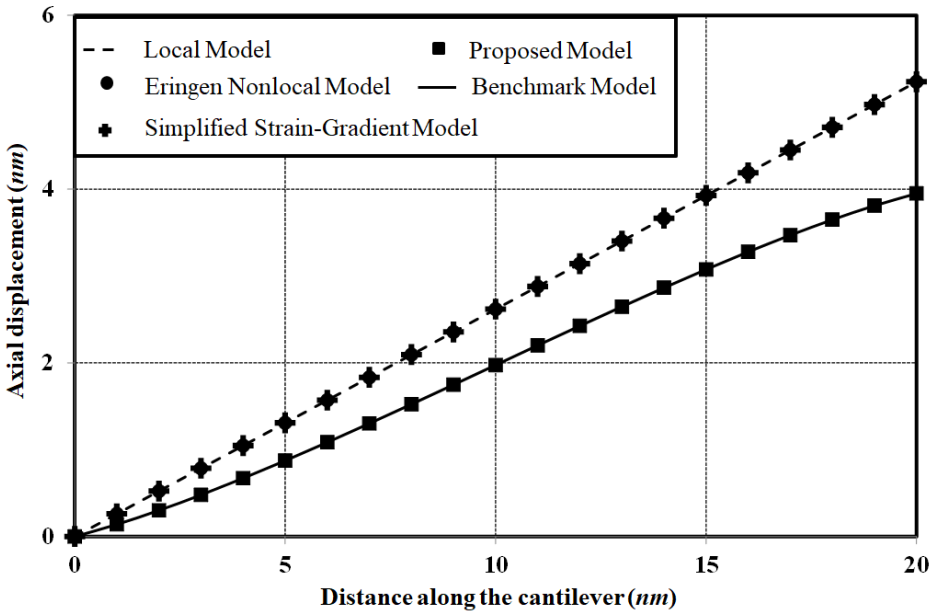

Fig. 6 Axial displacement versus distance along the cantilever under constant axial-force state

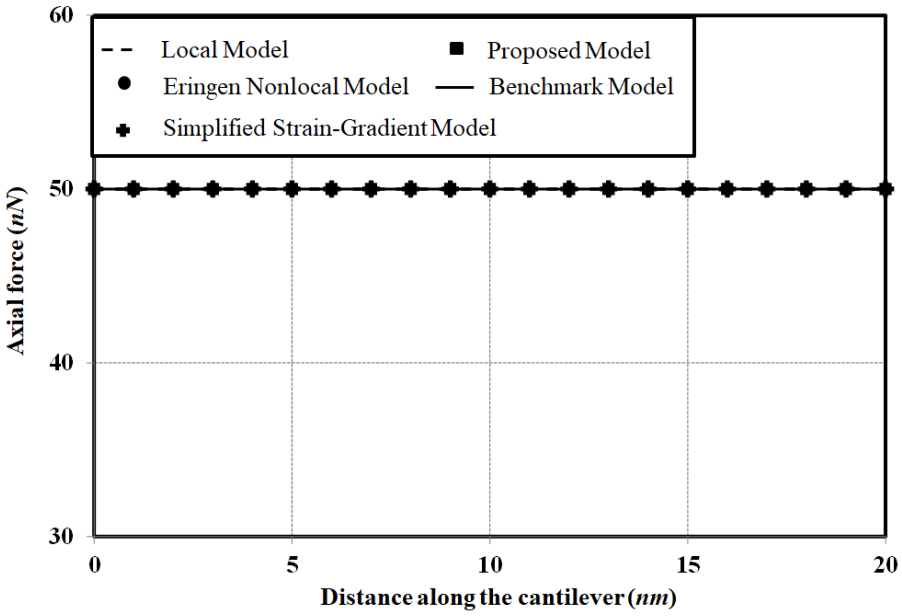

(a)

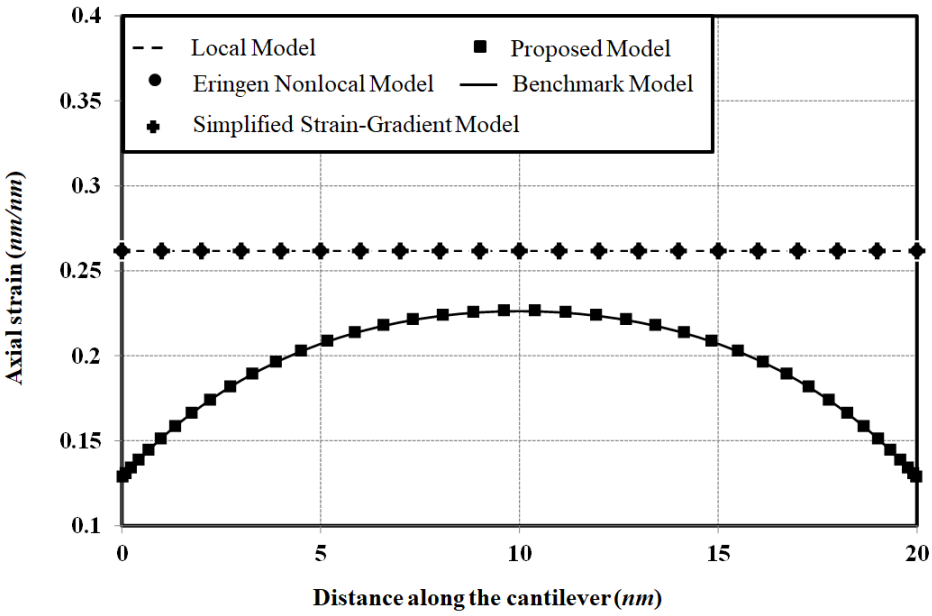

(b)

Fig. 7 (a) Axial force and (b) Axial strain versus distance along the cantilever under constant axial-force state

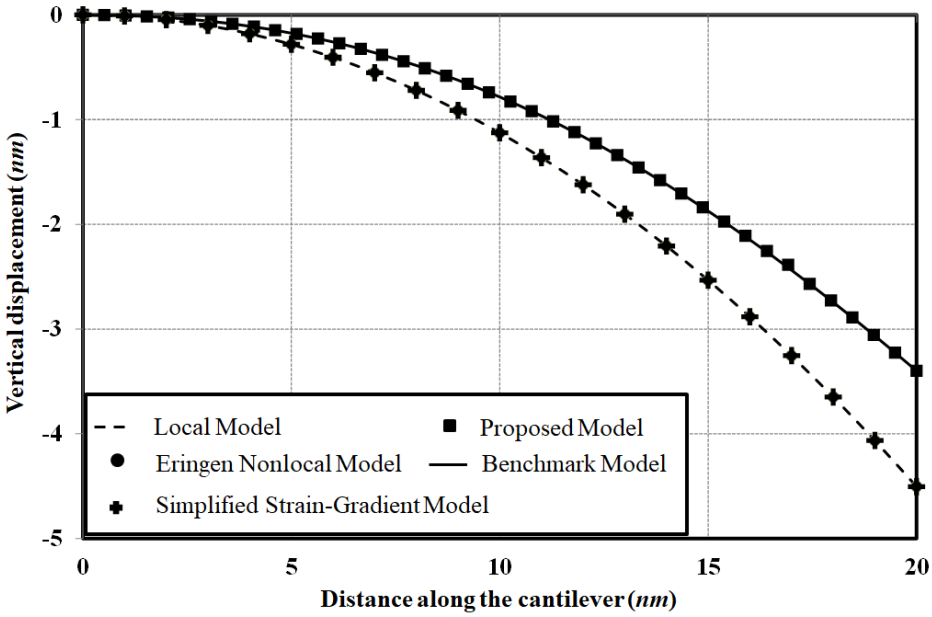

Fig. 8 Vertical displacement versus distance along the cantilever under constant bending-moment state

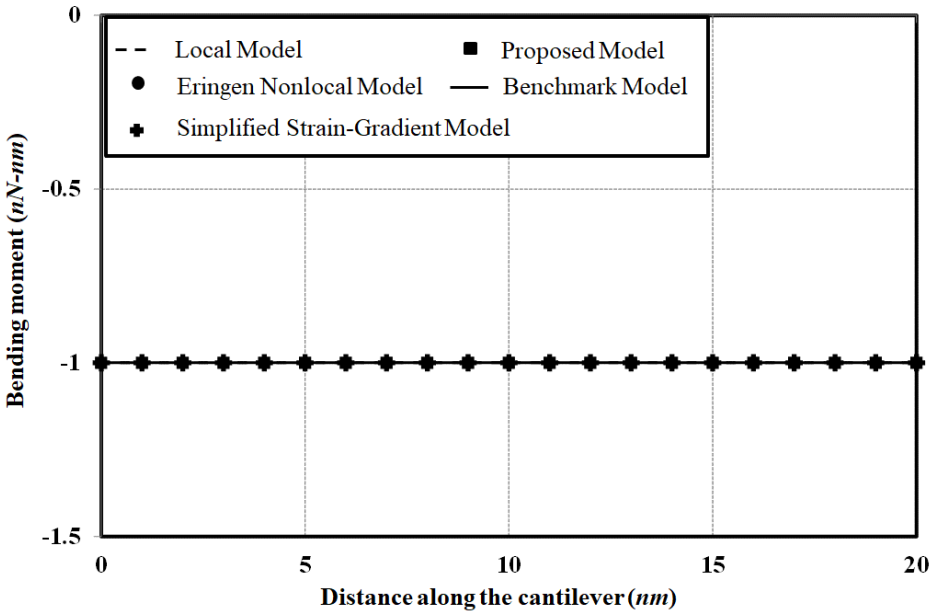

(a)

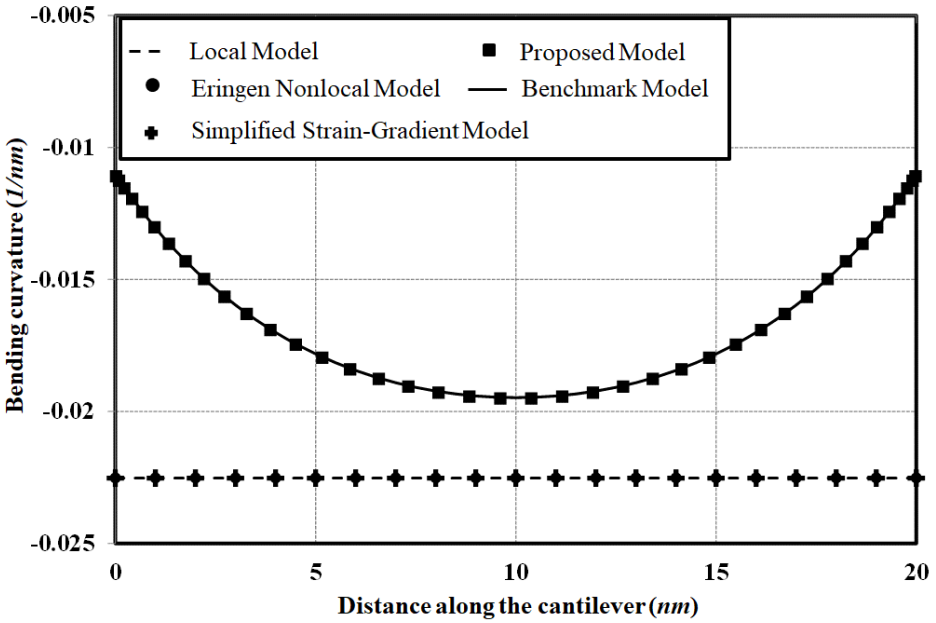

(b)

Fig. 9 (a) Bending moment and (b) Bending curvature versus distance along the cantilever under constant bending-moment state

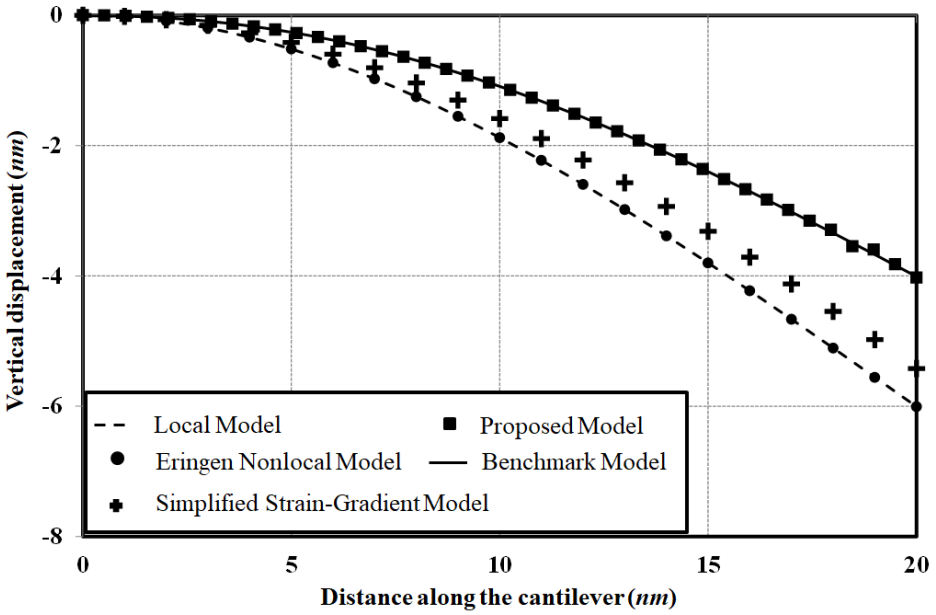

Fig. 10 Vertical displacement versus distance along the cantilever under constant shear-force state

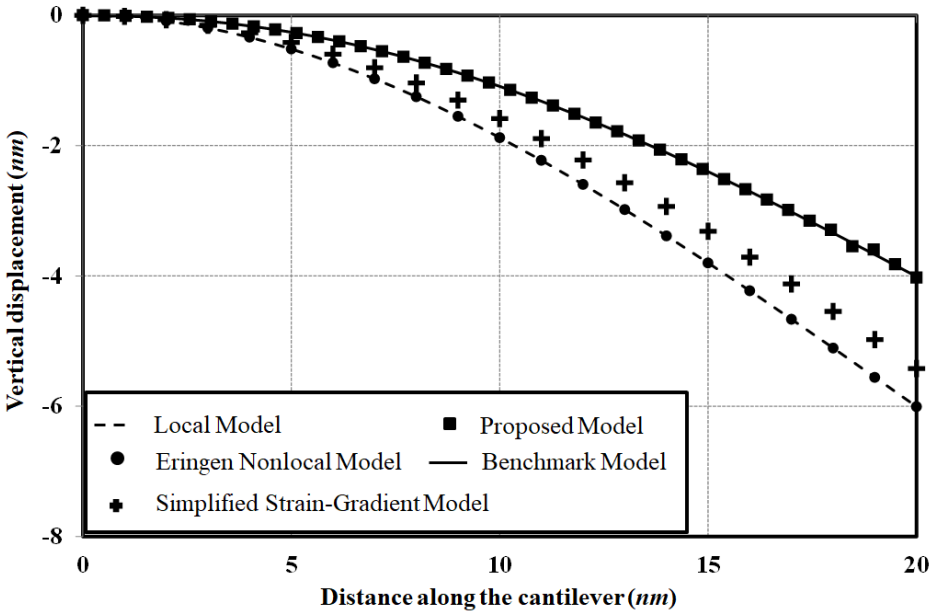

(a)

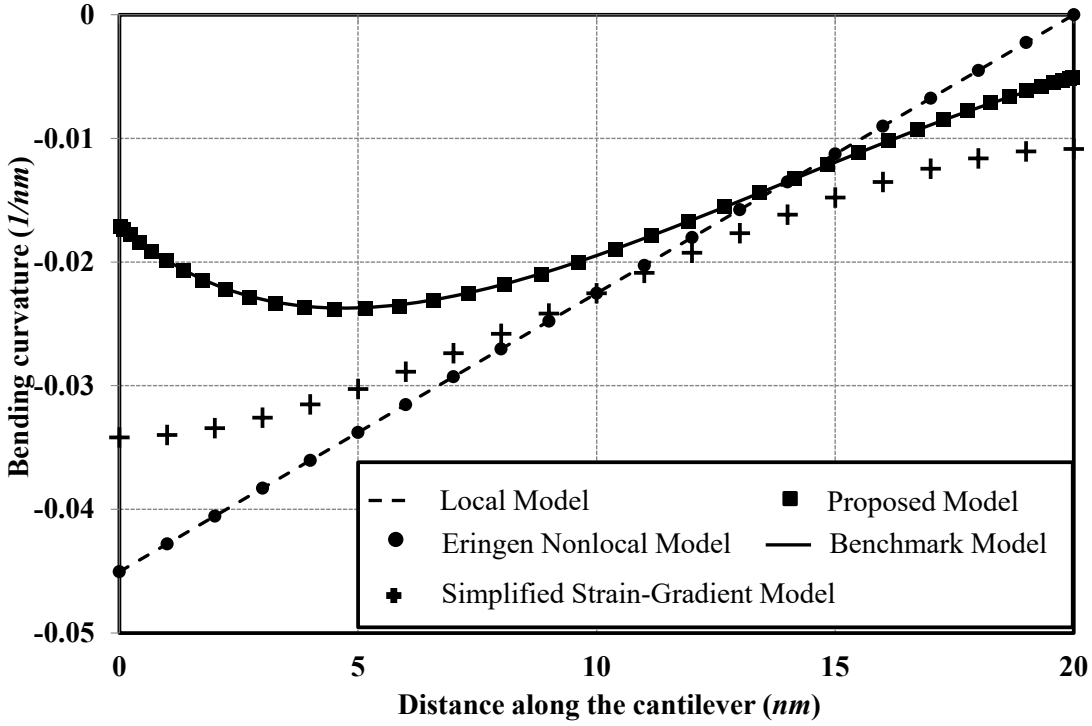

(b)

Fig. 11 (a) Bending moment and (b) Bending curvature versus distance along the cantilever under constant shear-force state

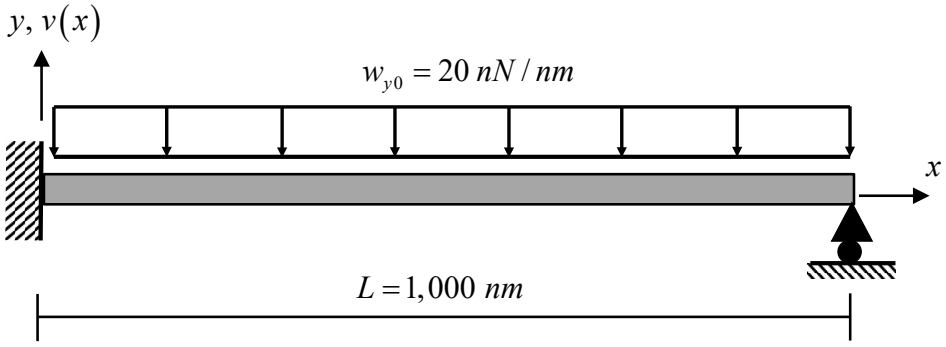

Fig. 12 Example II: a propped-cantilever iron nanobeam

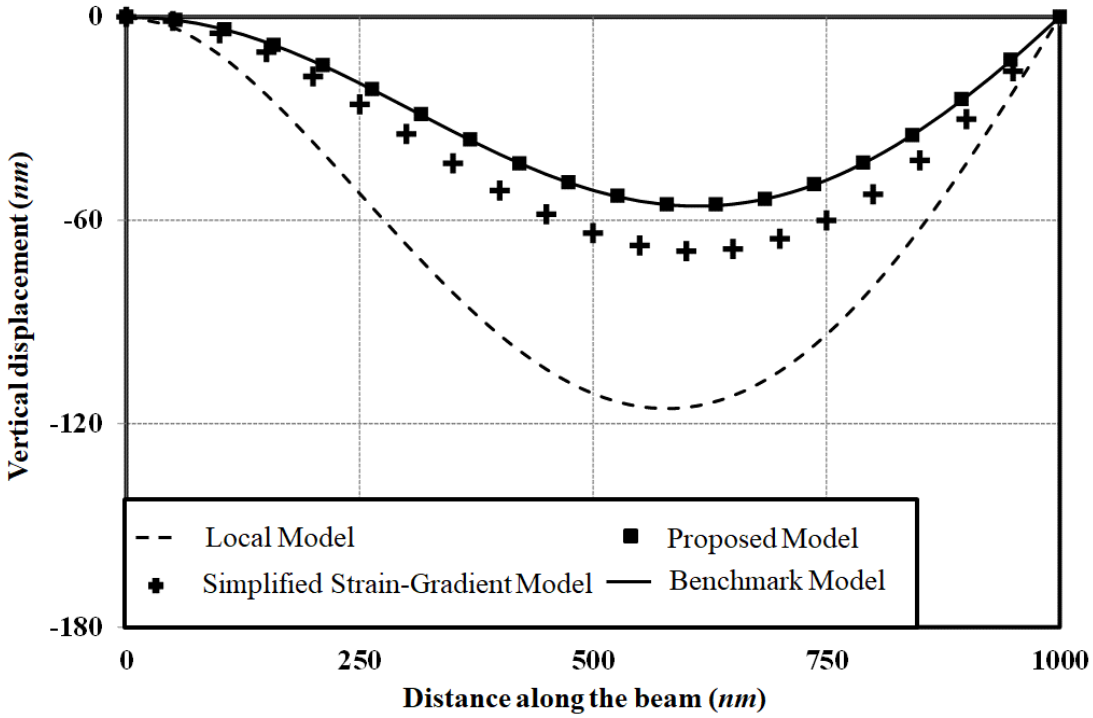

Fig. 13 Vertical displacement versus distance along the nanobeam

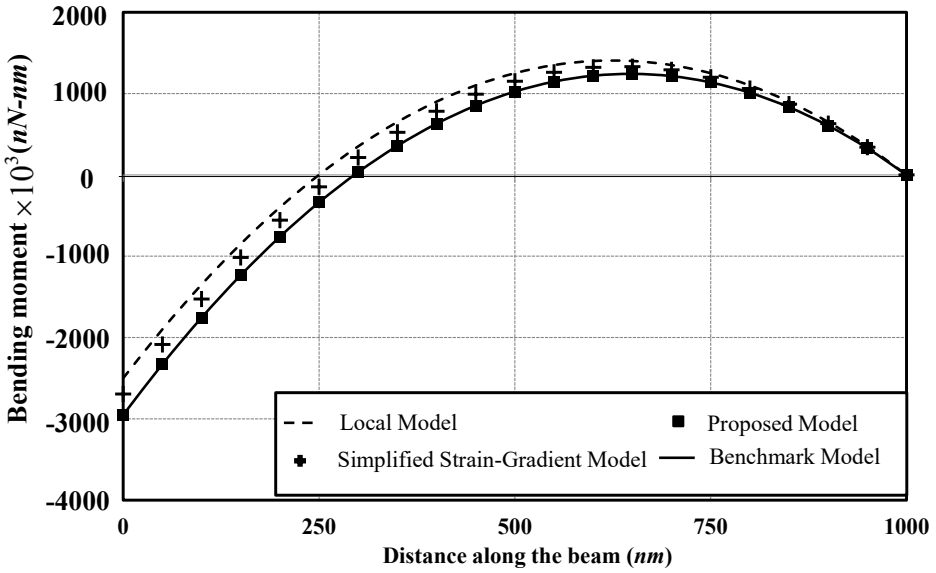

(a)

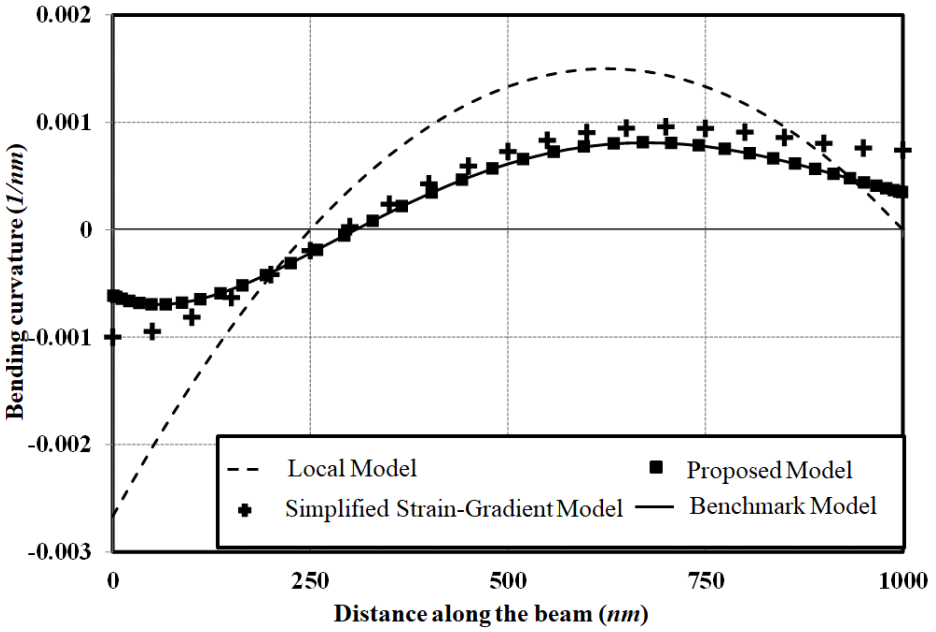

(b)

Fig. 14 (a) Bending-moment distributions; (b) bending-curvature distributions along the nanobeam

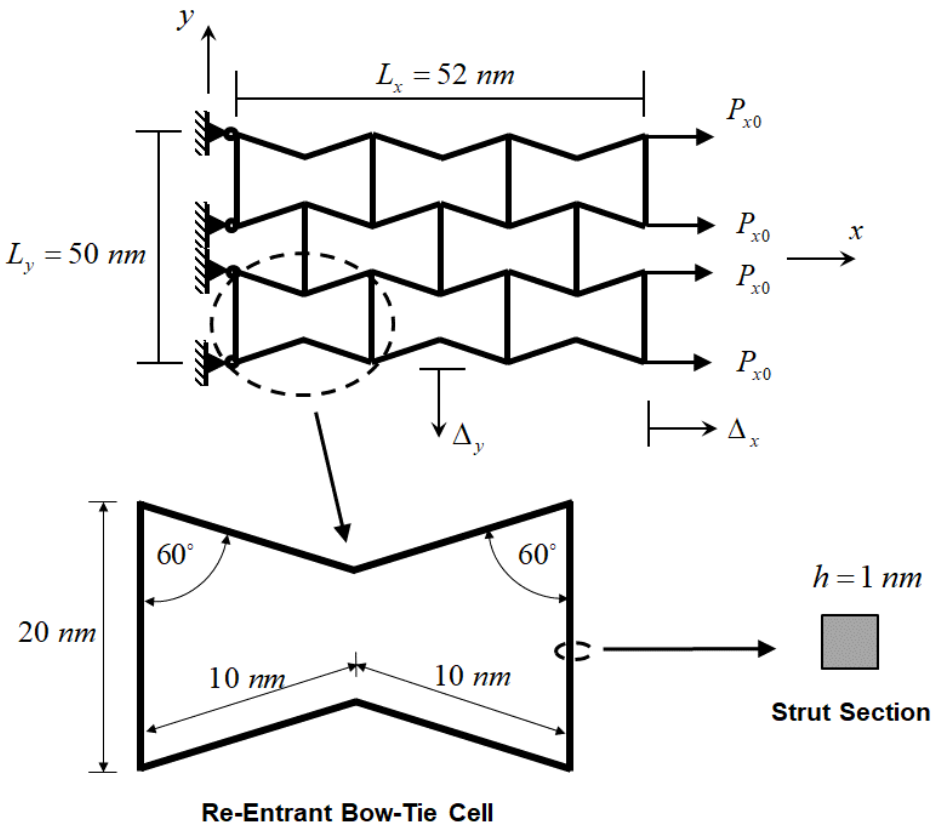

Fig. 15 Example III: quadrangular auxetic-metamaterial strip subjected to a tensile loading

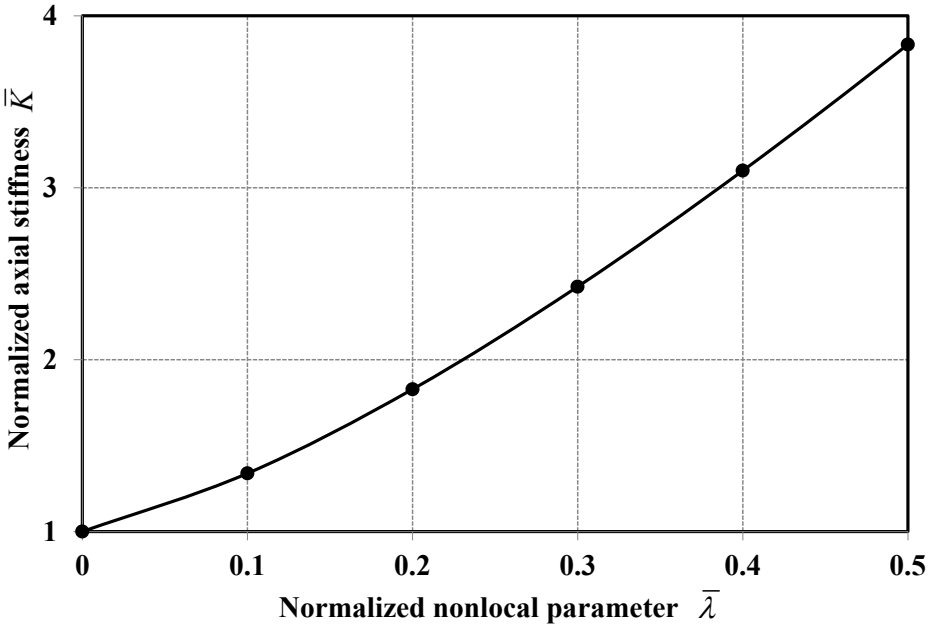

Fig. 16 Variation of normalized axial stiffness with normalized nonlocal parameter

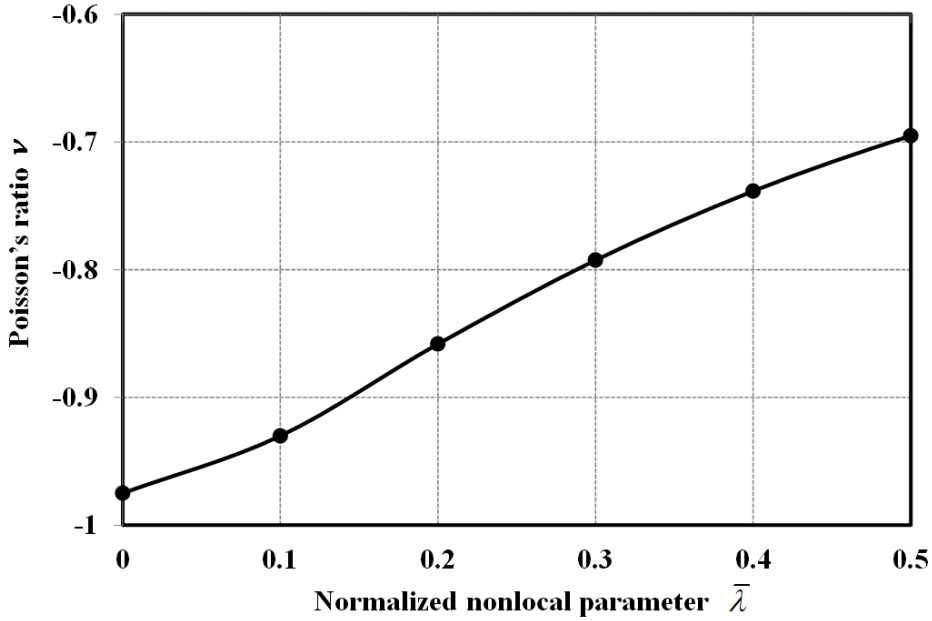

Fig. 17 Variation of Poisson's ratio with normalized nonlocal parameter